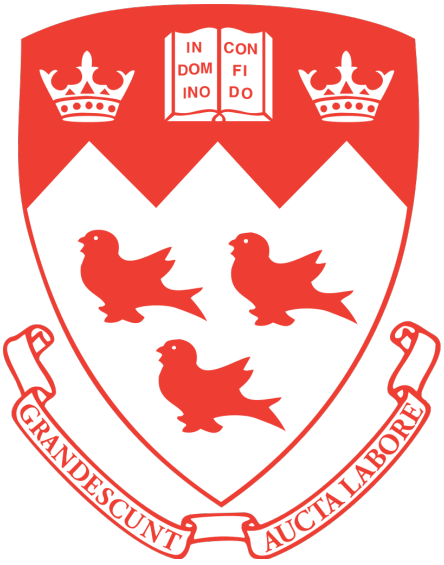

McGill University

Department of Mechanical Engineering

Montreal, Quebec

Particle Collection System for Turbulent Iron Fuel Burner

Martin Aralov

This thesis is submitted to McGill University in partial fulfillment of the requirements for the degree of Master of Engineering.

December 15, 2021

Abstract

Climate change is the largest global challenge of the 21st century. Combustion of fossil fuels for applications ranging from transportation to power generation is at the root of the issue. It is well known that when burnt, hydrocarbons release CO_2, CO, soot, and other harmful substances in the atmosphere that largely contribute to climate change. The Alternative Fuels Lab (AFL) has worked on solutions to this problem for the past few decades. Metal powder, particularly iron, is one of the proposed replacements of conventional fuels. This AFL project consists of proving the iron combustion cycle is a viable option as an alternative renewable and green fuel. After burning iron powder, the particles need to be collected to then be recycled and reused. The present work comprises of designing, manufacturing, and testing the collection system for the iron burner. The constraints for the separator are set both in terms of performance and of manufacturing, given its particular shape. Cyclone design models are employed to yield the most appropriate design for the task. The cyclone is then manufactured and coupled to the iron burner. Testing shows that the cyclonic separator is more than 99% efficient. The iron particles are then collected and analyzed. Different diagnostics are conducted on the unburnt and burnt powder. Scanning electron microscope, x-ray diffraction and thermogravimetric analysis are some techniques used to understand different aspects of the iron powder. They give insight on combustion efficiency, particle transformation and size changes throughout the process. Additionally, results on the performance of the system as a whole are presented, such as a heat extraction from iron flame. A second generation of the cyclone is designed and manufactured. It addresses some new desired improvements from the first iteration, such as the flow rates and heat retention. The second version of the cyclone is not extensively tested at the moment of writing this thesis.

Abrégé

Le changement climatique est le plus gros défi global du 21e siècle. L'utilisation de combustibles fossiles est omniprésente toutes les sphères de notre vie, du transport à la génération d'énergie, passant pas la production de biens. Le combustion d'hydrocarbures émet du CO, CO2, de la suie et d'autres substances nocives, contribuant majoritairement aux changements climatiques. Le Alternative Fuels Lab (AFL) à l'université McGill a travaillé sur ce défi pendant les dernières décénnies. Les particules métalliques, plus précisément de fer, sont une de solutions possible pour le remplacement des carburants conventionnels. Ce projet consiste à démontrer la possibilité durable de la boucle de combustion de fer comme un combustible alternatif, renouvelable et vert. Après étant brûlées, les particules doivent être récupérées pour être recyclées et reutilisées. Le présent travail comprend la conception, la fabrication et les essais du système de collecte pour le brûleur de fer. Les contraintes pour le système de séparation sont autant en termes de performance que de fabrication, vu sa forme particulière. Des modèles de conception de cyclones sont utilisés afin de rendre le résultat le plus convenable pour atteindre les buts. Le cyclone est ensuite fabriqué et couplé au brûleur de fer. Des tests montrent que le séparateur cyclonique est efficace à plus de 99%. Les particules de fer sont ensuite collectées et analysées. Différents diagnostics sont effectués sur la poudre brûlée et non brûlée. Le microscope électronique à balayage, la diffraction des rayons X et l'analyse thermo-gravimétrique sont des techniques utilisées pour comprendre les différents aspects de la poudre de fer. Elles donnent un aperçu de l'efficacité de la combustion, de la transformation des particules et des changements de taille tout au long du processus. De plus, des résultats sur la performance du système dans son ensemble sont présentés, comme l'extraction de chaleur de la flamme de fer. Une deuxième génération du cyclone est conçue et fabriquée. Elle répond à certaines améliorations souhaitées par rapport à la première itération, telles que les débits et la rétention de chaleur. La deuxième version du cyclone n'a pas été testée de manière approfondie au moment de la rédaction de cette thèse.

Acknowledgements

I would like to thank my Master's degree supervisor Professor Jeffrey Bergthorson for his support, guidance and constant presence throughout my degree. His patience and constructive criticism inspires students to always work harder and leave no stone unturned, to always strive to achieve their best.

I would also like to thank all the members of the Alternative Fuels Lab that were present during my time at the lab. I would like to particularly thank Samson Bowen-Bronet, Frederic Blais, Marie Meulemans, Jan Palecka, Keena Trowell, Santino Salvo, Antoine Durocher and Kartik Mangalvedhe for their support and help. Sam Goroshin provided expertise, knowledge and constructive criticism which improved my work and the final result of the project. I would like to extend recognition to the McConnell Engineering Building porter, Enrico Recine, who always welcomes you with a smile and gives unconditional and relentless support to the students. I would like to acknowledge the support from Natural Sciences and Engineering Research Council of Canada and Tata Steel Ltd. helping to fund my research and equipment for the project.

Finally I would like to thank my family, and particularly my parents who have always sacrificed their comfort and desires to provide the best for their children, and continue selflessly to do so. Ina and Denislav, I am forever grateful to you, and for the values you taught me.

Contents

List of Figures

List of Tables

1 Introduction

1.1 Motivation

Perhaps the biggest global challenge of the 21st century is climate change and the main reason for it are fossil fuel. From energy production, to transportation, heating and food processing, fossil fuels are an essential part of the global economy. Besides the obvious harmful emissions from fossil fuels, it is also estimated that the reserves are on the decline and that in the next 50-100 years, most of the energy produced could be extracted from clean primary sources [1, 2, 3, 4].The discussion about carbon-free energy sources has been going on for a few decades and many candidates are being put forward as a solution for the future: biofuels, hydrogen, solar, wind and nuclear energy are the most discussed ones. The more difficult task to overcome however is not the lack of energy availability: yearly there is more solar energy that reaches the Earth than the annual energy consumption of humans [3]. The challenge to solve is recreating the convenience of fossil fuels in terms of stored energy, ease of transportation and trade.

It has to be noted that solar, wind and hydro energy sources in fact do not offer energy storage as stand-alone systems. Wind farms for example convert wind energy into electricity, which has to be redistributed into the grid right away. The process is similar for solar farms and hydro-electric dams. The solution that first comes to mind is energy storage in batteries.

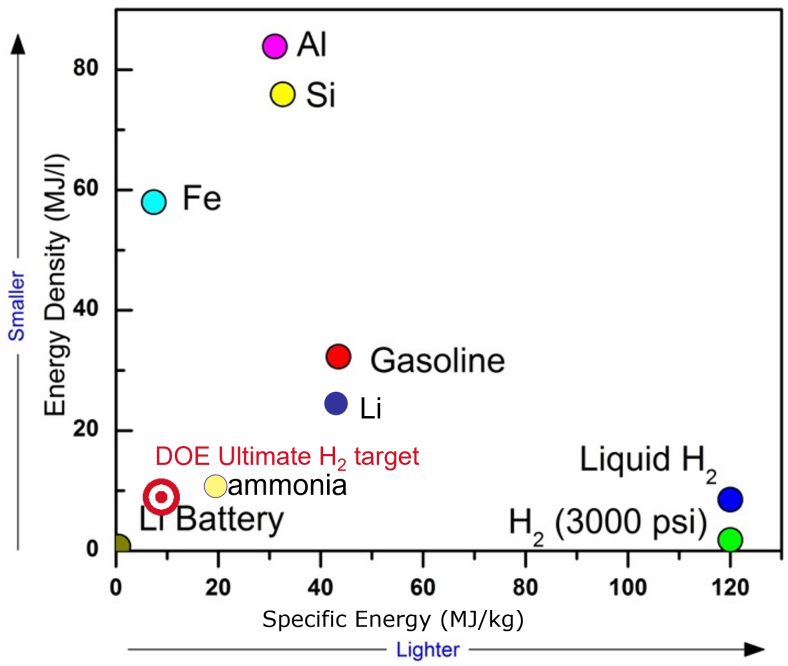

Figure 1.1: Energy Density vs Specific Energy of Certain Energy Carriers

As shown in Fig. 1.1, the energy density of lithium batteries is much lower than the one of fossil fuels; more than an order of magnitude lower. This is partly due to the fact that conventional batteries carry both the fuel and the oxidizer, increasing their weight, and thus reducing useful energy density [1]. Hydrogen fuel is convenient due to its high reactivity and its relatively easy incorporation in existing systems such as internal combustion engines, turbines and fuel cells [2]. There are however two major obstacles that hydrogen brings: the low density of compressed hydrogen and the hazardous properties such as fire and explosion.

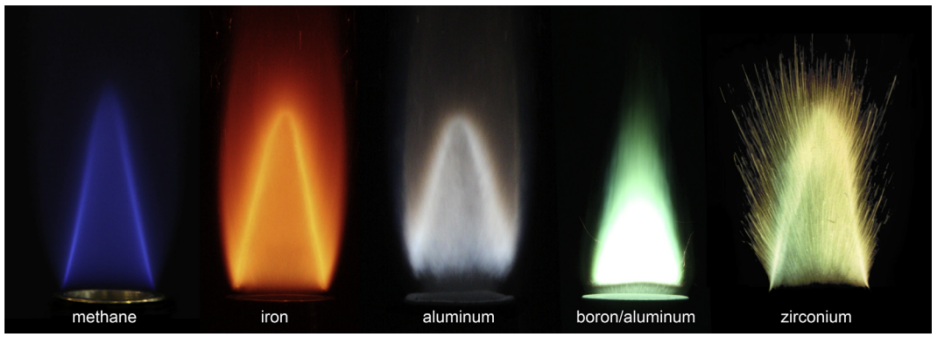

Figure 1.2: Stabilized Metal Flames on Custom-built AFL Bunsen Burner

Upon closer examination of Fig. 1.1, it is seen that metals have similar specific energy and energy density values as gasoline (and other fossil fuels). In fact the Alternative Fuels Lab has been working towards the development of direct metal combustion and metal-water combustion. When metals react with oxygen, whether in air or water, they produce a stable, nontoxic solid oxide in a carbon-free exothermic reaction, a combustion process. Once burned, the metal oxide particles must be collected to be regenerated (reduced), which is the topic of this thesis and the challenge solved by this project. Metals' high abundance, high reactivity when oxidized, high energy density and stability in ambient conditions makes them perfect candidates for renewable fuels [1, 2].

The AFL has already performed multiple metal combustion experiments. Metal flames are stabilized using custom-built Bunsen burners (seen in Fig. 1.2) and custom-built counterflow burners [5, 1]. Metal combustion experiments have also been performed in a hele-shaw cell, and onboard a rocket and parabolic flights to achieve micro-gravity environment [6, 7, 8]. Most of those experiments are performed to study fundamental properties of metal flames. The current project differs by the fact that it is a proof-of-concept study rather than a set of fundamental experiments.

To understand why metal powder, and particularly iron, is a suitable candidate for direct combustion with air, one has to examine the combustion of single particles in the heterogeneous flow, that is iron and air (the oxidizer). Firstly, it is assumed that metal particles are to be combusted in a

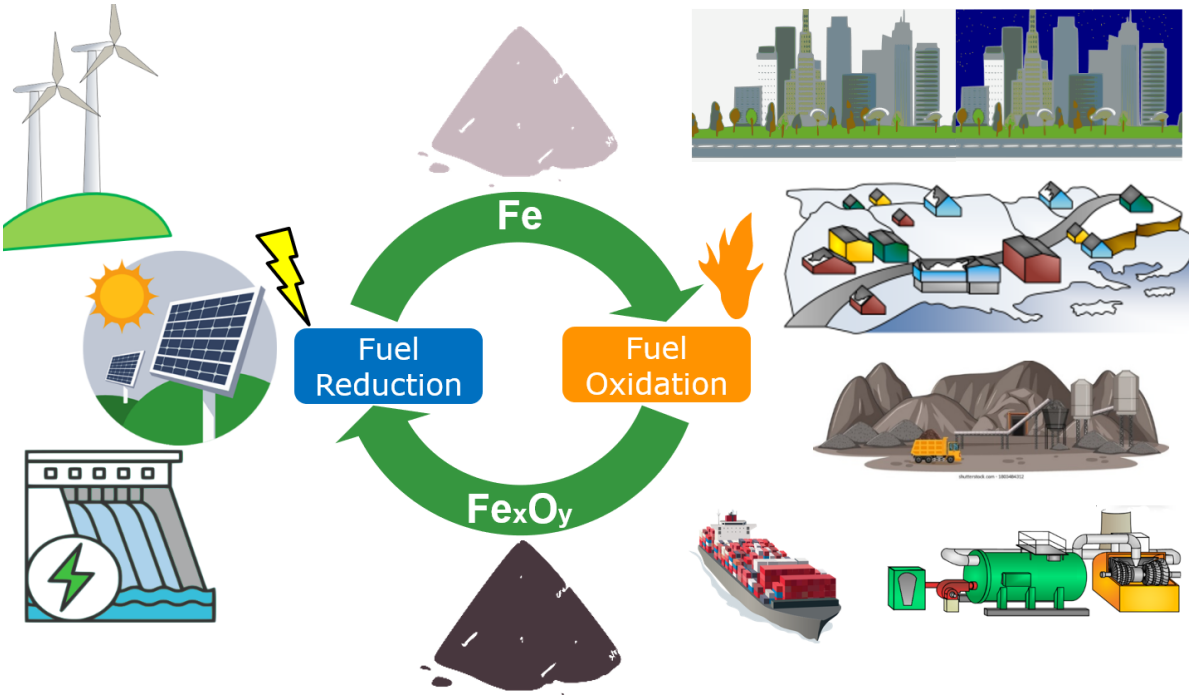

Figure 1.3: Proposed Conceptual Iron Fuel Cycle

small Biot number regime, given that the particles are small, which means internal temperature gradients are negligible [9]. The Biot number is the ratio between thermal conductivity inside a body, due to conduction, and the thermal conductivity to the outside, through the surface of that body, due to convection. It is given by eq. (1.1), where it can be seen that if the conductivity k of the particle is larger than the convective heat transfer coefficient h, the Biot number will be small. R is a characteristic dimension, in this case the radius of the particle, which is small, and also contributes to a small Biot number. The Biot number examines the heat transfer inside the particle, which is radial, and so the characteristic dimension is the radius.

$$Bi = \frac{h}{k}R \tag{1.1}$$

The convective heat transfer coefficient h is related to the thermal conductivity of the fluid k_f by the Nusselt number:

$$Nu_D = \frac{h}{k_f}D \tag{1.2}$$

The Nusselt number has the diameter of the particle D as a characteristic dimension, since it is a relation of the heat flow at the boundary in the fluid, the boundary being the particle surface.

Rearranging eq. (1.2) to isolate h and substituting it in eq. (1.1), one obtains:

$$Bi = \frac{Nuk_f}{k_s}\frac{R}{2R} = \frac{Nuk_f}{2k_s} \tag{1.3}$$

It is known for small spherical particles that the Nusselt number can be approximated to 2 [10]. Thus only the ratio of thermal conductivity of the fluid to the thermal conductivity of the solid is what will determine the value of the Biot number, which is small in the case of metal particles because they have a much higher conductivity than air.

There are then three possible combustion modes in which the particle can burn, shown in Fig. 1.4. The combustion mode is determined by whether the flame temperature of the metal-fuel mixture with the oxidizer (in this case air), at a stoichiometric ratio, is above the boiling point of the metal or not [11]. Furthermore, the flame temperature may be limited by the evaporation or dissociation point of the combustion products, since evaporation of said products would absorb heat and limit the flame temperature increase [11, 1]. A good example of metal particles that burn in Mode A, the vapor-phase droplet combustion, is the combustion of magnesium. Wang et al. show that the calculated adiabatic flame temperature for magnesium is 2586K whereas the boiling point is much lower, at 1363K. This results in a vapor-phase droplet combustion and the formation of nano-particles on the surface of the combusted particles [12, 13]. As for iron combustion, the adiabatic flame temperature for iron combustion in air is 2250K whereas its boiling point is much higher at 3130K [14]. The expected mode of combustion is narrowed down to Mode C, meaning iron and iron alloys do not burn in a vapor phase; the oxidation takes place at the surface of the molten mixture[15, 16]. The iron oxide formation results in metal-oxide solid particle formation that is larger and heavier than the initial metal particle, as explained by Bergthorson et al [1].

The aim of this work is to achieve a very important step in this quest for a new generation of carbon-free fuel systems — a self-sustained iron flame particle collection system. Previous work from the AFL, or anyone else, has not been able to achieve a purely self sustained iron flame, without either the addition of a pilot flame or hot products. Additionally, this system needs a collection system for the iron particles being oxidized in the burner so that they can be collected and recycled. The full cycle of iron oxidation begins by introducing a mix of iron and air in a self-sustained burner. The heat produced by the combustion process is then harvested for direct usage or electric conversion by a heat cycle. The carbon-free exhaust is directed towards a collection system which separates the iron oxide particles from the gaseous flow. The particles are collected,

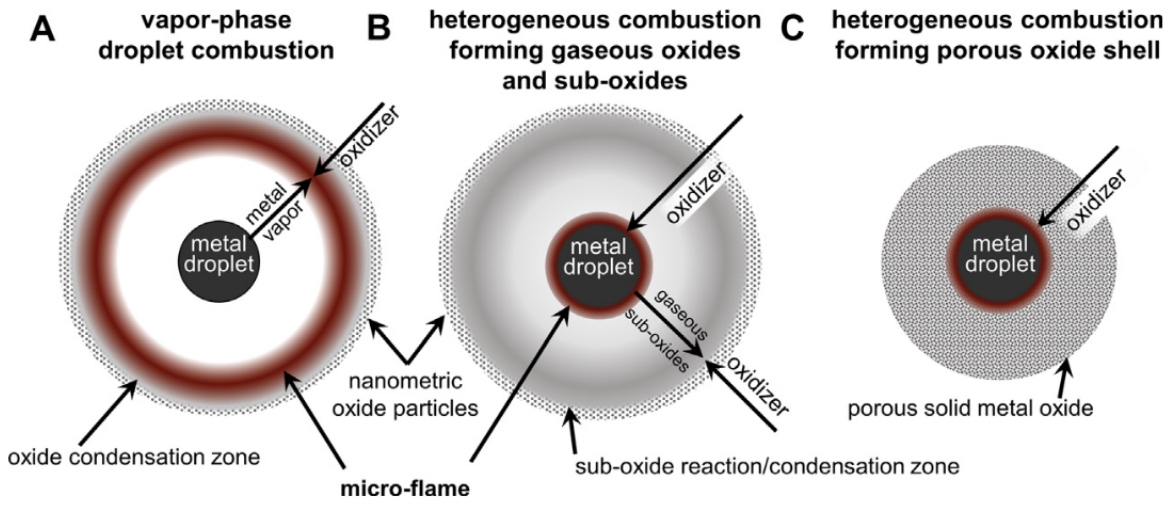

Figure 1.4: Combustion Modes of Metal Particles in the Small Biot Number Regime [1]

and analyzed. They are reduced using primary energy, such as solar or wind energy, when it is in excess. This is how energy is stored into the iron, which can then be reintroduced in the burner and re-combusted for energy extraction.

In essence, the iron particles become an energy storage solution. The abundant renewable energy is stored in iron during the reduction process, and is released on demand, when the iron is burned. Similar to batteries, iron fuel becomes a reusable and transportable energy source. A comparison can also be made to hydrogen production by water electrolysis. Renewable energy is used to produce hydrogen fuel in a carbon-free process, which is then burned without producing greenhouse gases [17, 18]. Iron fuel however is safer and more energy dense than both of those energy storage solutions. A conceptual illustration of the iron fuel cycle is shown in Fig. 1.3.

1.2 Project Objectives

This project is a collaboration between two Master's students, working on two parts of the system: the self-sustained burner and the collection system. This work will present the work done on the collection system and combustion products analysis. The objectives are to:

1. Continuously separate the combusted particles from the heterogeneous post-burner flow, resulting in a clean exhaust flow;
2. Collect the said particles in order to perform oxidation reduction on them;
3. Evaluate the collection system performance, in terms of collection efficiency;

4. Analyze the combustion products in order to evaluate the burner performance and give insight on processes occurring in the system.

The main challenge of the collections system is that the particles to be separated need to be unaltered in order to be useful for the next steps of the process. Though this will be later discussed in detail, most separation devices and methods interact with the solid particles, which results in a physical or chemical alteration, or a difficult or impossible retrieval. An additional challenge is the state of the iron particles in the post-burner region, being hot and abrasive and thus not suitable for all separation techniques. Finally, a high collection efficiency is required in order to truly complete the iron fuel cycle.

The first step to achieve these goals is to understand and select and appropriate separation device for the system. The device is then to be designed and fabricated, in parallel with the design and manufacture of the burner. The laboratory space of the AFL is the destination of the burner-collector system, and thus the assembly must fit in the smallest footprint possible, with a maximum height of 2 metres. Multiple tests and experiments will then be performed, beginning by stabilizing a self-sustained iron flame. The collection efficiency of the separation is to be evaluated by comparing quantitatively the mass of particles collected to the mass of particles dispersed. Once the products are retrieved, they will also be subject to multiple tests. The main topic of interest is the nature of the oxide formation and the level of oxidation. Finally, attempts for heat extraction from the burner will be made.

2 Background

2.1 Separation Devices

Cyclones are devices that separate solid particles from a fluid flow. This is achieved by exploiting the density difference between the solids and the carrying fluid — solids are usually denser than fluids. Cyclones exert centrifugal forces to the heterogeneous flow, which results in the solid particles hitting the side wall of the cyclone, reducing their tangential velocity to zero, and making them slide to the bottom where the collection container is. The fluid follows the flow paths and exits the cyclone, particle free [19, 20]. Solid particle can be removed from fluid flows for multiple reasons, such as but not limited to: removal of harmful particles, use of particle for a subsequent process, or simply for their value, for resale. Of course cyclones are not the only method for removing particles from a flow. The reader is probably more familiar with other methods such as filters, but the cyclone has its particular advantages that are necessary for the AFL burner-cyclone assembly. Filtering is one of the most efficient methods for removing particles from a flow. Filter are usually made from a cloth-like material with pores of known size. When a filter is inserted in a heterogeneous flow, it does not let the solid particles larger than the pores pass through it. The advantage of this device is high efficiency and high reliability of separation [21, 22]. However, as particles build up on the filter as they cannot pass through, the pressure drop through it increases. Additionally, the openings get saturated and the filter starts retaining smaller particles. When it is deemed that the filter is full, it needs to be cleaned or replaced. Usually the particles retained in the filter fibers cannot be fully extracted as they are stuck to the fibers, or at least they cannot be retrieved without being altered. Furthermore due to the type of materials used for filtering, this method cannot be used in high temperatures processes (250°C at most) [23]. Because filters are consumables, retain particles in them, cannot be used in high temperatures or in aggressive environments, they are not suitable for the burner-cyclone process.

Wet scrubbers are another separation technique used in industry. They are particularly useful for smaller sized particles, where conventional methods of particle removal are not as efficient [24]. In wet scrubbers, liquid droplets are sprayed directly in the incoming flow. The droplets stick to the dust due to its high inertia, increase its weight and diameter and make it easier to collect. Wet scrubbers can be combined with other systems, such as cyclones and settling chambers. Advantages of wet scrubbers are that there is no pressure loss in the process and that it is an efficient solution for very fine particles (less than $1\mu m$). However the major drawback for this project is

the contamination of the iron particles with the scrubbing liquid (usually water). Firstly, the water can chemically alter the particles by oxidizing them. This is unacceptable since the collected products need to be unaltered as much as possible, physically and chemically. The products are to be further analyzed and reveal information on the burner performance and processes happening inside the system. Secondly, when using liquid scrubbers, the heterogeneous gas flow become heterogeneous liquid flow, an iron powder slurry. This makes the powder retrieval difficult, if not impossible. Liquid scrubbers are then unsuitable for the burner-cyclone system.

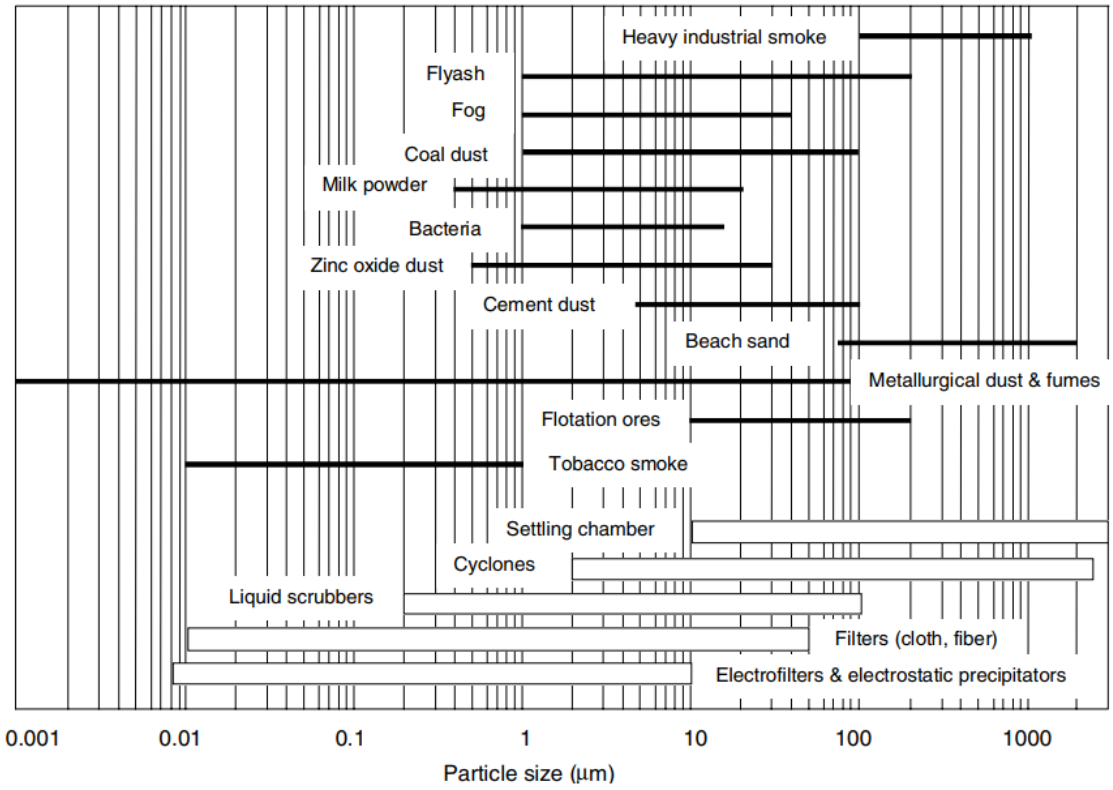

Figure 2.1: Different materials, their particle size range and the appropriate separation devices [23]

Settling chambers are one of the simplest separation devices. When a gas-solid mixture flows slowly through the device, the higher density particles (solids) settle on the bottom of the chamber, simply due to gravity. To achieve this effect, the settling chambers need to be big in size to allow enough time for particles to slow down and fall downwards. Additionally, settling chambers are mostly efficient for larger particles, above $500\mu m$ [23]. Because flow needs to be slowed down or stopped in a settling chamber, and because they are not efficient for the particle size associated with this project, this method is not suitable for the process.

Cyclones are considered the most suitable separation device for this project. With the proper

design, the cyclonic separator addresses the exact particle size range that is to be tested in the burner-separator system of the AFL. Cyclones specifically exploit the density differences of the components of heterogeneous flows, as is the case of the burner exhaust. They have no moving parts and they require low to no maintenance, given there are no consumables in the system. The noninvasive separation of solid particles allows for high fidelity and authenticity of the iron powder as it comes out of the burner, which in turn leads to meaningful testing and analysis. Finally, cyclones are relatively easy and cheap to manufacture, making them fitting for a quick and inexpensive first iteration of a burner-separator system. For those reasons the cyclone is selected as the particle separator and collector of choice to be paired with the AFL turbulent iron burner.

2.2 Cyclones

The first feature of a cyclone is the overall type and shape of the device. The two shape configurations of the cyclonic separating devices are the cylinder-on-cone cyclone and the cylindrical cyclone. The inlet configuration heavily dictates its performance, and the most common inlet types are depicted in Fig. 2.2. The first one, the pipe inlet, is the cheapest and easiest one to manufacture. It is mostly used in applications where performance can be sacrificed or where the separated solids are relatively large (wood shops, grain processing). The second type, the slot inlet, is the most common type of cyclone. They are also called tangential since they direct the inlet of the flow to the perimeter of the cyclone's cylindrical body, in contrast with the last type, the axial inlet. Slot inlet cyclones are relatively easy to manufacture and yield good separation performance. The third type of cyclone is similar to the slot inlet, the wrap-around inlet. The increased diameter at the inlet creates a higher inlet angular momentum due to the increased spin velocity. This type of cyclone is mostly used in higher capacity systems. It allows for increased solid loading and gas flow, without increasing the cylinder and cone diameters and lengths. Finally the fourth inlet type is the axial one. It is used with cylindrical cyclones, and multiple of those are configured in an array. Their advantages are that they create lower pressure losses than cylinder-on-cone cyclones, since the flow has minimal changes in direction (and thus in momentum). They are however less efficient in separating particles, and the vanes require complex machining.

The dimensions that define the cyclone geometry, depicted in Fig. 2.3, and that are the design variables are:

- Body diameter (D)

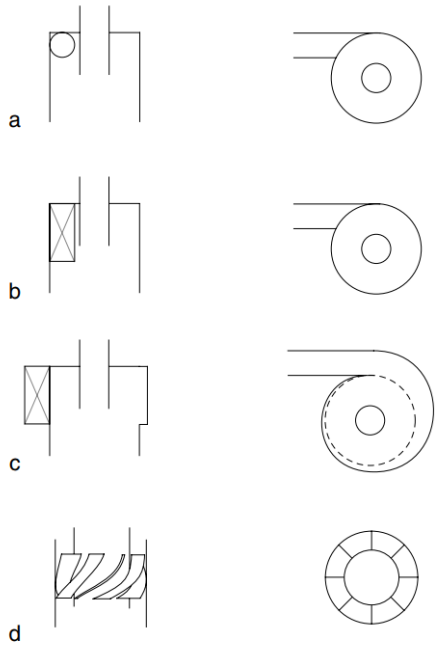

Figure 2.2: Types of cyclone inlets: a. pipe inlet, b. slot inlet, c. wrap-around inlet, d. axial inlet with swirl vanes [23]

- Total height (H)
- Diameter of the vortex finder (D_x)
- Length of the vortex finder (S)
- Height and width of the inlet (a and b)
- Height of the conical section (H_c)
- Diameter of the powder exit (D_d)

The dimensions influence different flow parameters of the gaseous and solid flows in the cyclone. For example, an inlet of smaller dimensions speeds up the flow (for the same flow rate) and increases pressure drop (due to increased friction). A larger cylinder diameter reduces the tangential flow velocity, which reduces the change in momentum and thus the centrifugal forces.

The separation efficiency together with the losses through a cyclone (pressure drop) are the device's two most important characteristics. Quantifying the pressure drop of a cyclone is crucial since it determines the necessary power to drive the system. In cases where fine dusts are handled, the efficiency is the driving factor, but the pressure drop is still a primary design concern. Since

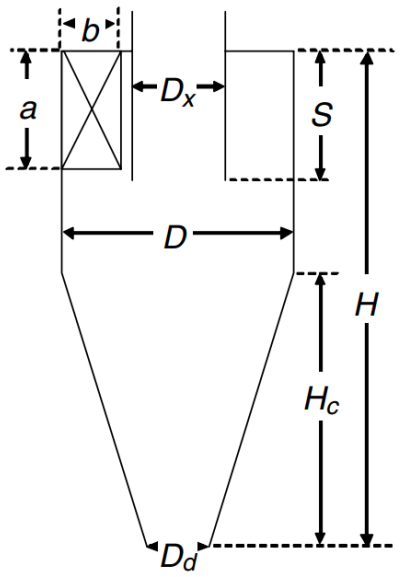

Figure 2.3: Slot Cyclone Dimensions [23]

cyclones have been subject to studies for nearly 100 years, empirical methods were predominant for understanding cyclones, until the modern digital age. The glass cyclone setup of Shepherd and Lapple allowed them to record and confirm flow patterns and pressure drop data inside the cyclone, while also examining particle patterns. In fact, prior to this work, the only theoretical expression for computing the pressure drop of a cyclone was applicable to cyclones with fixed dimensional proportions and a linear velocity distribution exponent for the flow velocity inside the cyclone [25]. Instead, Shepherd's work concluded that the velocity distribution exponent should instead be $n = 0.5$ and was able to yield a friction loss equation that had cyclone geometry as variables, instead of only one fixed size ratio [26]. The friction loss, F_{cv}, is a non dimensional factor expressed as the number of cyclone inlet velocity heads. The expression is shown in eq. (2.1) where r_a, r_0 and r_d are derived from the cyclone's entry dimensions, outlet diameter, and the depth of the outlet tube inside the cyclone (S) [26].

$$F_{cv} = \frac{r_a}{\sqrt{r_0 r_d}} \tag{2.1}$$

The friction loss, F_{cv}, also expressed as ΔH, is an expression of the energy loss inside the cyclone, as a factor of the inlet velocity of the cyclone. For a given cyclone design, ΔH is a constant factor for all inlet velocities. The higher the inlet velocity of the cyclone, the higher the pressure drop through it. The correlation between the pressure drop ΔP in [Pa] and ΔH is shown in eq. (2.2)

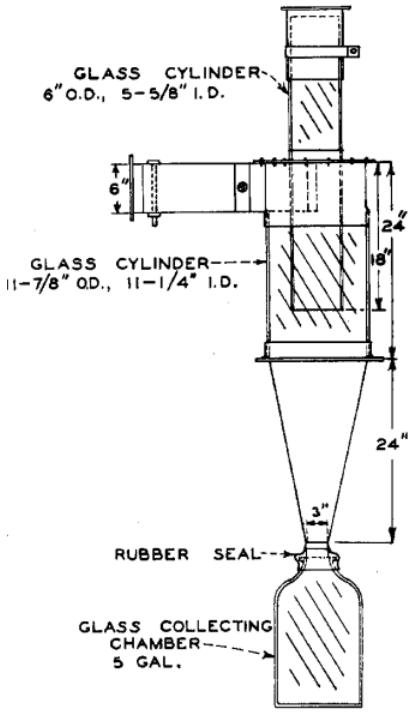

Figure 2.4: Glass Cyclone Setup of Shepherd and Lapple Fig. 2.4

related by the inlet velocity v_i and the gas density ρ_g [27, 28].

$$\Delta P = \Delta H \frac{\rho_g v_i^2}{2} \tag{2.2}$$

Leith and Mehta's work from 1973 [29] evaluates different cyclone models that were developed up to that point in time. Theoretical values from the friction loss equations (ΔH) from Shepherd and Lapple (1939) [26], First (1950) [30], Stairmand (1949) [31] and Barth (1956) [32] are all compared to experimental pressure drop values. The conclusion drawn is that the Barth, Stairmand, and Shepherd and Lapple methods correlate best with experiments, however the Shepherd and Lapple approach is the simplest and thus preferred method, the one shown above. [29].

Although since the 1930's, cyclones were considered to be the separation devices of choice for particles above $10\mu m$ [26], different cyclone collection efficiency models are also evaluated in Leith and Mehta's work. Before getting into the cyclone efficiency models, the underlying mechanism of particle separation needs to be introduced.

The flow inside the cyclone is separated in two components: the gas flow pattern and the particle flow. Overall, the separation occurs because the particles cannot "keep up" with the gas flow. This is due to the large difference in density between the two components of the flow — gas and solids.

The fluid particles follow the flow patterns in the cyclones seen in Fig. 2.5 , which are determined by the pressure differentials and the shape of the cyclone. The pressure in the vortex finder, the outlet of the cyclone, is lower than the one in the inlet. This is achieved by either sucking the flow from the outlet, or pushing it in through the inlet. The geometry of the cyclone itself directs the flow in a downward spiral on the outside, to then come back up through the middle. The height of the vortex finder, being below the inlet, prevents the flow from doing a bypass, which means going directly from the inlet to the outlet without following the flow paths. While the flow is carrying the solid particles, they do not experience the same forces as the fluid particles. The fluid particles are subject to equal and opposite radial forces seen in Fig. 2.8: the outward one is the centrifugal force due to the rotational change in momentum while the inward one, the resultant pressure force, is due to the pressure differentials in the cyclone which create the flow paths.

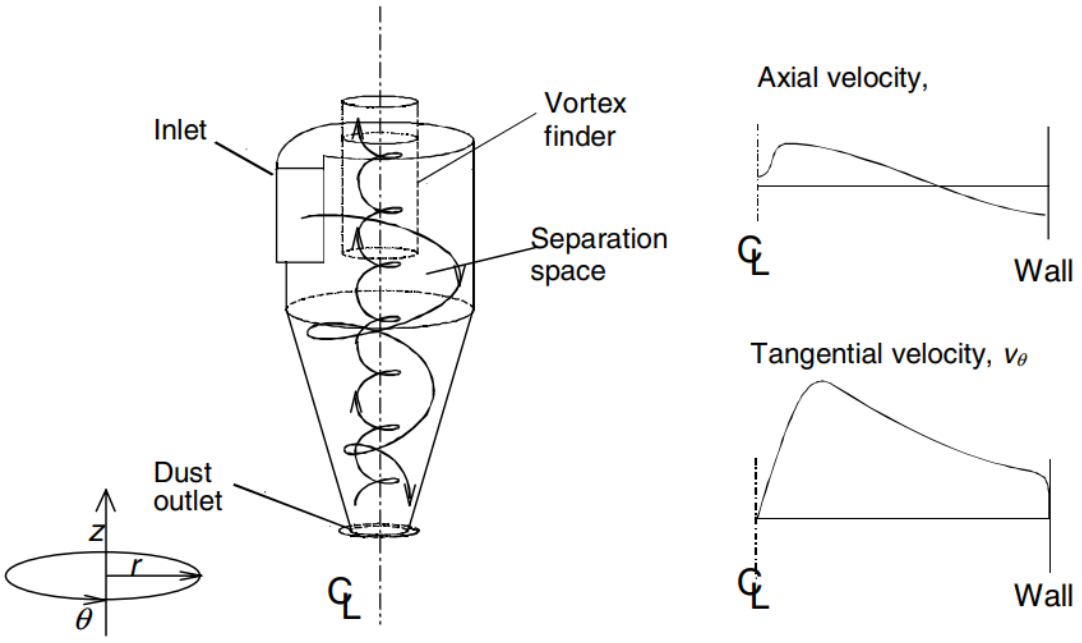

Figure 2.5: Flow Patterns and Gas Velocities in a Tangential Entry Cyclone [23]

In fact, the particles in a cyclone are almost always moving at their terminal velocity, relative to the gas, and so they can be "limited" in terms of following the gas flow. Simply put, the terminal velocity is determined by the body force on a particle and the drag acting on it. The time scale in which the particle reaches its final velocity is also critical since it will delay the particle motion. The terminal velocity of a given particle in turn determines if the particle is separated or passes through the cyclone [23]. Given the low density of the fluid (ρ), and the small particle diameter

(x), the Reynolds number of the particle relative to the flow around it is also low:

$$Re_p = \frac{\rho||\boldsymbol{U'}||x}{\mu} \tag{2.3}$$

Here $\boldsymbol{U'}$ is the particle velocity relative to the flow (as a vector), and the Stokes' regime can be assumed for the frictional, or drag, forces acting on the particles [23, 33, 19]. A terminal velocity equation for the particle in the radial direction can then be found, using Stokes' law, and substituting the gravitational force by the centrifugal force as they are deemed to be comparable. So for cases where the density of the particle is much larger than the density of the gas ($\rho_g >> \rho$), which is the case of the heterogeneous flow inside cyclone separators, the equation is as follows [23, 29, 27]:

$$U'_r = v_{Stokes} = v_{ts} = \frac{d^2\rho_p}{18\mu}\left(\frac{v_\theta^2}{r}\right) \tag{2.4}$$

Here above d is the particle diameter and $\frac{v_\theta^2}{r}$ is the centrifugal acceleration in terms of tangential velocity and radius from the center of the cyclone. However a crucial, non-dimensional relation is found from Barth's studies in 1956 between the particle's terminal velocity and a critical terminal velocity for a given flow [32]. The idea is that for a critical particle diameter, the centrifugal forces are balanced by the drag forces [27]. These particles that keep their path on a fixed radius and do not move neither to the wall nor the center of the cycle are considered "static" particles. The settling velocity equation for the static particle is given by:

$$v_{ts}^* = \frac{Qg}{2\pi h^* v_\theta^2} \tag{2.5}$$

In the equation h^* is a geometrical property of the cyclone. The ratio of v_{ts}/v_{ts}^* then determines whether a given particle will travel radially to the wall of the cyclone, or towards the centre of it. Once again substituting the gravitational acceleration g with the centrifugal one, the ratio is [29, 27]:

$$\frac{v_{ts}}{v_{ts}^*} = \frac{\pi h^* v_\theta^2 d^2 \rho_p}{9\mu Q} \tag{2.6}$$

A ratio of 1 means that particles will remain on a fixed radius path and will not move toward the cyclone wall nor the center. Thus the diameter for which the ratio is 1, is the critical diameter of the particle, commonly referred to as d_{50} or x_{50}. If the ratio is above 1, the particles have

a radial velocity larger than the critical one and will be ejected toward the wall of the cyclone, and consequently be separated. The higher the ratio, the higher the chance of a particle is to be collected by the cyclone, as it is shown in Fig. 2.6 and Fig. 2.7. In fact the critical diameter is called d_{50} because there is a 50% chance for a particle of that diameter to be separated.

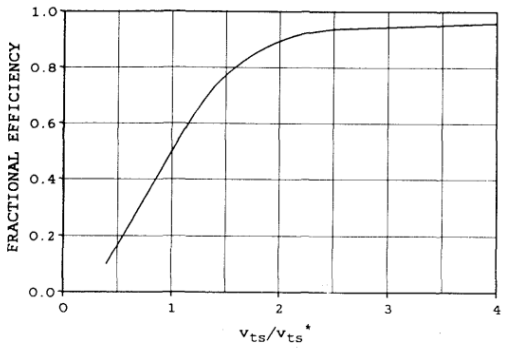

Figure 2.6: Fractional Collection Efficiency vs Critical Velocity Ratio [27]

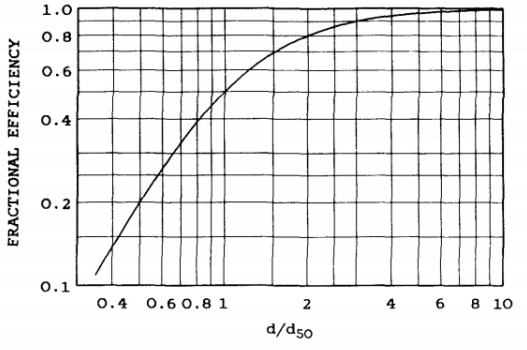

Figure 2.7: Fractional Collection Efficiency vs Critical Diameter [27]

In short, the drag forces created by the relative slip velocity between the gas flow and the particles, combined with the solids' higher density, contribute to an inequality in the pressure and centrifugal forces. For large enough particles, the net forces in turn push the particles outwards towards the walls of the cyclone, creating a net U_r, as seen in Fig. 2.9. There, the particles hit the wall, lose their tangential velocities, and fall downwards toward the collection bin. The particles are not re-entrained into the flow once they reach the cyclone wall, because at the wall itself there is a boundary layer with a tangential velocity of zero, shown in Fig. 2.5. As a counter example, small enough particles are able to keep up with the fluid flow and will eventually escape the cyclone through its outlet together with the gaseous flow.

An analogy of this phenomena can be made with passengers in a moving car. The car, being the gas flow, carries its passengers with it, the solid particles. When the car takes a sharp turn (the gas entering the cyclone), the passengers experience a centrifugal force pushing them towards the outside of the curve. The centrifugal force for the gas particles is balanced by an equal and opposite pressure force, keeping the gas, or the car, in its track. However, the particles are subject to forces that are not balanced, as are the passengers in the car, which are pushed to the opposite side of the turn direction. When the particles hit the wall of the cyclone, they fall downwards and are collected.

Leith and Mehta's work evaluates the correlation of the performance of cone-under-cylinder cyclones

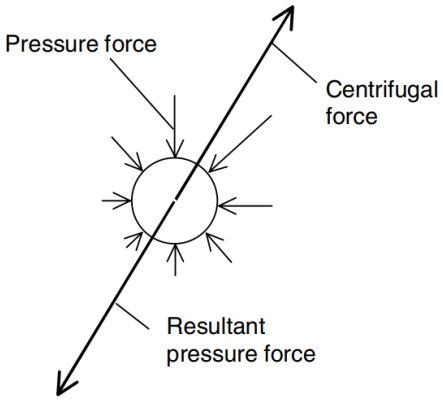

Figure 2.8: Radial Forces on a Rotating Fluid Element [23]

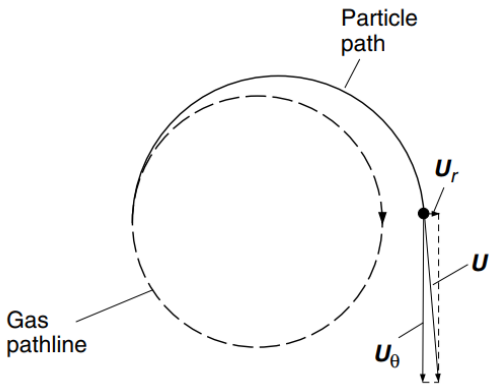

Figure 2.9: Solids Particle Path Deviating from the Fluid [23]

to different design models previously developed. Besides evaluating cyclone design models, the paper also gives an introduction to the basic operation concept of a cyclone. It is mentioned that cyclones are excellent separators for particles around and larger than $5\mu m$ [29]. The basic design method for a cyclone is by predicting its collection efficiency, using design models. The models usually relate the dimensions of the cyclone to its diameter, as shown later in table 3.1, and the diameter is determined by design parameters. In contrast with high throughput cyclones, the high efficiency models process about half as much volumetric flow, for the same dimensions and pressure drop. High efficiency cyclones generally produce higher pressure drop for the same amount of flow as a high throughput separator. After evaluating cyclone performance and comparing it to different prediction models, it is concluded that the Stairmand model, and its improvement, is one of the better models. Furthermore, it is concluded that the first generation of design models do not take into account all relevant factors to a cyclone's performance, they rather concentrate on only one goal: efficiency, pressure drop, flow rate, etc. [29]

In the following decades, scientists started building up on the cyclone models from the 50's. The modern cyclone designs' performance could no longer be predicted by the models developed, and thus a need for more intricate theories arose [33]. Dietz' work explored a model that takes into account cyclone geometry, recognizes the importance of turbulent flow inside the cyclone and does not assume that the core region (the middle of the cyclone) and the annular region (closest to the periphery) are well mixed. The approach taken is to separate the cyclone into three regions, shown in Fig. 2.10, and estimate the flux of particles Γ between the zones with the following differential equations.

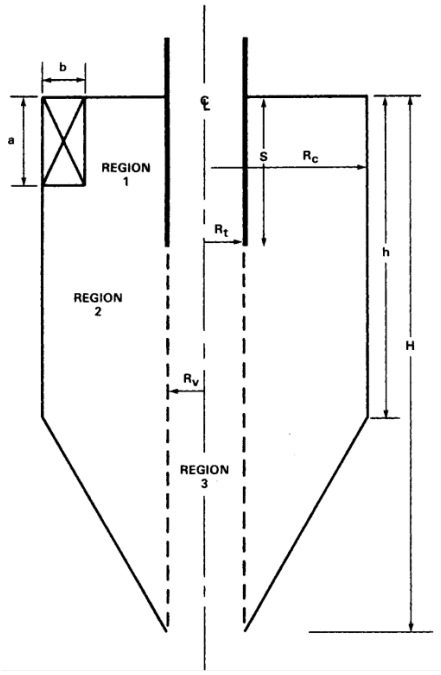

Figure 2.10: Sketch of the Regions Modeled by Dietz [33]

For the particle flux from Region 1:

$$\frac{d}{dz}[Q_{v0}n_1] = -2\pi R_c \Gamma_u(z) \tag{2.7}$$

For the particle flux from Region 2:

$$\frac{d}{dz}[Q_v(z)n_2] = -2\pi R_c \Gamma'_u(z) - 2\pi R_v(z)\Gamma_v(z) \tag{2.8}$$

And for the particle flux from Region 3:

$$-\frac{d}{dz}[Q_v(z)n_3] = 2\pi R_v(z)\Gamma_v(z) \tag{2.9}$$

The z axis is downward, starting from the top of region 2 to the bottom of the cyclone. The particle flux from regions 1 to 2 is considered to be 100% of the particles, since they have nowhere else to go, assuming no bypassing of particles occurs. So then the fluxes of interest are the flux to the cyclone wall $\Gamma'_u(z)$ and the one to the cyclone core (region 3) $\Gamma_v(z)$. In fact if the flux towards region 3 is known, the flux towards the cyclone wall is also known since those two compose the complete mass flow rate of particles. Thus Dietz found that Γ_v is given by eq. (2.10), where U_r is the radial velocity of the gas carrying particles to the core region and the centrifugal forces pushing

particles outward with velocity U_{pv}.

$$\Gamma_v = n_2 U_r - n_3 U_{pv} \tag{2.10}$$

Solving the differential equations, and applying the inlet conditions, Dietz finds expressions for the axial concentration profiles in the three regions, n_i to be [33]:

$$n_1(z) = n_0 \exp\left[\frac{-2\pi R_c U_{pu'}(z+D)}{Q_v}\right] \tag{2.11}$$

$$n_2 = n_{1(z=0)}\left[1 - \frac{z}{l}\right]^{\beta} \tag{2.12}$$

and

$$n_3 = n_{1(z=0)}\left[\frac{A-\beta}{C}\right]\left[1 - \frac{z}{l}\right]^{\beta} \tag{2.13}$$

where

$$\beta \equiv \frac{1}{2}[A - 1 - C] + \frac{1}{2}[(C - A - 1)^2 + 4AC]^{1/2} \tag{2.14}$$

$$A \equiv \frac{2\pi R_c l U_{pu'}}{Q_v} \tag{2.15}$$

and

$$C \equiv \frac{2\pi R_t l U_{pv}}{Q_v} \tag{2.16}$$

Details of the derivation and the variables are found in Dietz's paper, *Collection Efficiency of Cyclone Separators*[33]. Implementing and evaluating the multiple region idea and considering turbulent mixing, Dietz's model showed promising results. After a comparison with experimental values, the model proved to be more accurate than previous models, such as Stairmand and Lapple, particularly for smaller particle sizes [33].

It is conceptually quite simple to determine a cyclone separator's overall collection efficiency. The total particle mass flow incoming into the cyclone ($\dot{m}_i$) is composed of the mass flow of particles captured ($\dot{m}_c$) and the mass flow of particles that escape the device ($\dot{m}_e$).

$$\dot{m}_i = \dot{m}_c + \dot{m}_e \tag{2.17}$$

Rearranging the terms to obtain the collection efficiency η:

$$\eta = \frac{\dot{m}_c}{\dot{m}_i} = 1 - \frac{\dot{m}_e}{\dot{m}_i} = \frac{\dot{m}_c}{\dot{m}_c + \dot{m}_e} \tag{2.18}$$

Assuming the values of the mass fractions are known, efficiency η is found. This expression however does not reveal information about which particles get collected and which escape, in terms of particle size. Thus the separation characteristics of a cyclone are better represented by its grade-efficiency curve (GEC). The GEC gives information about the separation efficiency of particles with a diameter x:

$$f_i(x)dx = \eta f_c(x)dx + (1-\eta)f_e(x)dx \tag{2.19}$$

where $f_i(x)$ is the inlet fraction of particles with diameter x, and $f_c(x)$ and $f_e(x)$ are the fractions of collected and escaped particles respectively. Applying the fractions to the mass fractions, the separation efficiency η for a diameter x can then be found:

$$\eta(x) = \frac{m_c f_c(x)dx}{m_i f_i(x)dx} \tag{2.20}$$

When the efficiency function $\eta(x)$ is integrated over the diameter distribution of the solids sample, or practically speaking numerically solved with some small dx, it yields a grade-efficiency curve. This curve gives complete information about the cyclone separation performance. If one knows the solid particles size and distribution, they can predict the collection efficiency of the device. An example of a grade-efficiency curve is seen in Fig. 2.11. The x_{50} mark on the plot indicates the diameter of the particles that have 50% chance of being collected, or that escape the cyclone separator, as discussed earlier. This is the single most important characteristic of a cyclone, since it is the "cutoff" diameter. It is considered that any particle size below x_{50} escapes the cyclone.
As discussed earlier, the flow characteristics inside the cyclone determine whether the solid particles are to be separated or not. Particles' final velocity, particles load, the balance between centrifugal and drag forces, the pressure drop that influences the flow paths, and other parameters all play a role in determining the cutoff size, for a given flow. Thus, the grade-efficiency curve of a cyclone is not unique. The GEC changes shape and moves along the x-axis (cutoff diameter) with different

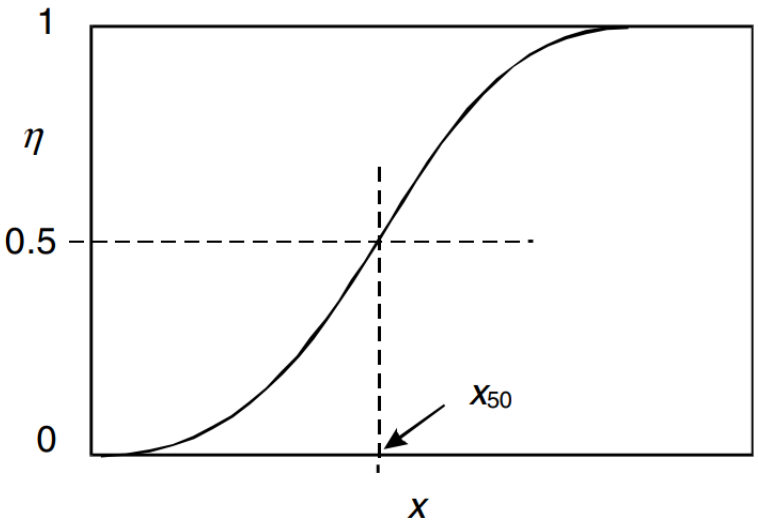

Figure 2.11: Typical GEC of a Cyclone [23]

flow properties and loads of solid particles with respect to the fluid. Furthermore, since the slope of the curve can be designed to be very steep, the x_{50} diameter can become a very clear-cut cutoff point, like a sieve. In such a design, a particle very slightly larger than x_{50} can be subject to a separation efficiency of nearly 100%.

The heterogeneous, 3-dimensional, multi-parameter, turbulent flow in the cyclone makes it extremely complex, if not impossible, to solve analytically. For the purposes of this project, a mix of different components from different models is used for the cyclone design, calculations and analysis. The models developed over the years are used in industry and have proven to be reliable and accurate. The calculations and design steps employed in the process are discussed in detail in section 3.4. The most practical model for designing cyclones to this day remains the Mushelknautz Method (MM). It is based on the work by Barth and has been constantly improved in many different aspects [23]. This is the method employed in this work, as presented in its latest form by Hoffmann and Stein in *Gas Cyclones and Swirl Tubes*.

Cyclone development continued with more and more specific work, sometimes related to the installations around the cyclone. An example is Abrahamson et al. study in 2002 where they evaluate different entry duct configurations for cyclone dust collectors. This is particularly interesting for this project since there is a length of ducting between the burner and cyclone, as it can be seen later on. In general, their work shows that the entry direction and velocity of the flow can significantly influence the cyclone's collection efficiency. Although the study cases are too many to generalize and it is best to compare a given design to Abrahamson's work examples, there are a few

general advice. One should avoid bends close to the cyclone, particularly those that push powder towards the inside wall of the inlet. Up-flow bends close to the cyclone which push powder close to the roof of the cyclone are also to be avoided. Long horizontal entry ducts are to be promoted immediately before the cyclone [34]. An example of some preferred and poor entry sections for a cyclonic separator is shown in Fig. 2.12.

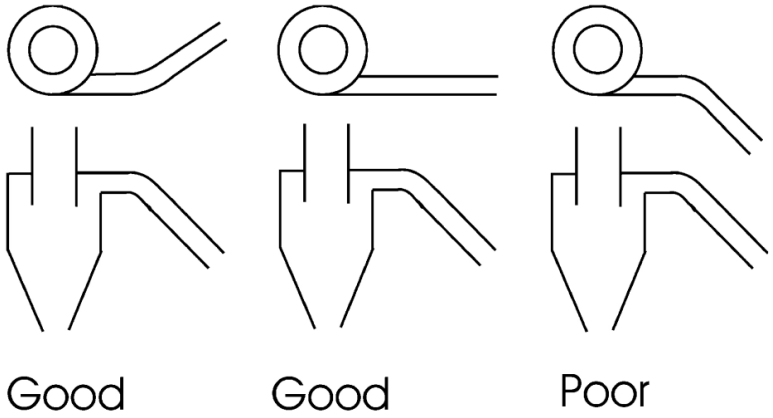

Figure 2.12: Example of Preferred and Poor Cyclone Entry Sections [34]

Continuing the idea of conditioning the flow before its entrance in the cyclone, Misyulya looked at an entry device to decrease the power consumption of a cyclone. The pressure loss inside the apparatus depends mainly on the rotary gas flow and loss in kinetic energy of the outlet vortex flow. Furthermore, it also depends on the cyclone geometry and the inner walls surface [35]. Fukui et al. study the effects of a porous metal cone, instead of a smooth resin one, on the inside of the cyclone. The experiment consists in injecting clean air through the pores and evaluating the separation efficiency as well as powder deposits on the wall. If clean air is not fed through the pores of the cone, the new design yields a inferior performance to the smooth surface one, both in terms of cut size and particle sintering. However for a specific flow rate of clean air, the cut size of the cyclone was decreased, resulting in a higher collection efficiency [36]. This research is useful for this project in terms of general design parameters and could be particularly useful when the first iteration design is to be optimized.

With the availability of computational power through computer models, research on cyclones is conducted with the help of Computational Flow Dynamics (CFD) simulations. CFD provides insight of mechanisms happening inside the cyclone, but is also computationally expensive compared to mathematical and empirical models [38]. Elsayed and Lacor developed a computational model

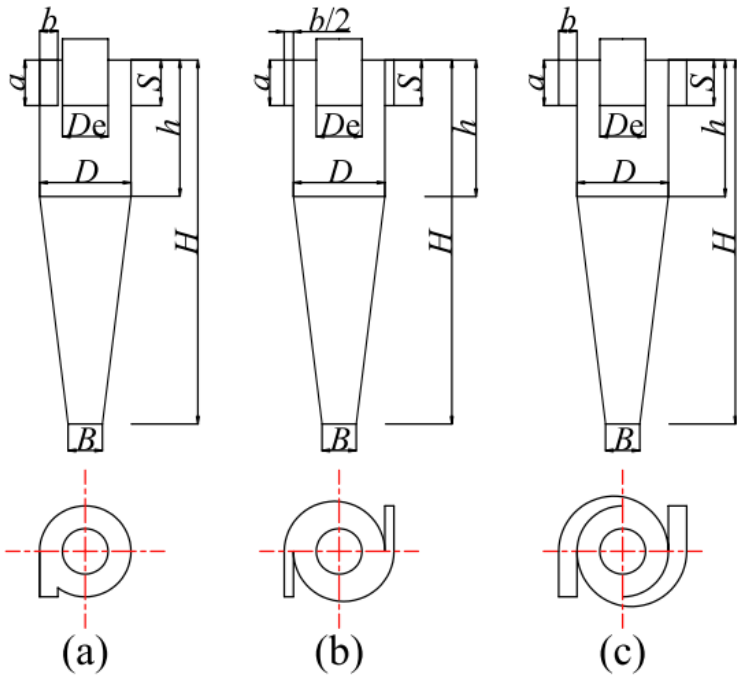

Figure 2.13: Symmetrical Spiral Inlets to Improve Performance Proposed by Zhao et al [37]

that uses response surface methodology (RSM) and CFD simulation to design a cyclone with a lower pressure drop. With RSM basically being a multi-parameter study, and the CFD analysis showing the meaning of the parameter changes, their study is able to reduce the pressure drop through a cyclone design by half [38]. There is not however a significant efficiency improvement. Another very similar study is by Sgrott et al, *Cyclone optimization by COMPLEX method and CFD simulation*. A cyclone design is first proposed by a multi-objective optimization and is then evaluated by CFD and compared to an existing model [39]. There are even studies that optimize the optimization methods, by identifying the relevant parameters to be evaluated as well as the relevant ranges [40]. A very interesting observation is that most of the computational methods use the Muschelknautz Model (MM) introducted by Hoffman as their base design. Some are able to improve the collection efficiency or cutoff diameter, but it is not a significant improvement in most cases [38, 39, 40]. This means that the MM is perhaps the best model one can use for a first iteration design. Additionally, given the objective of this work is to design and build a cyclone rather than modeling cyclones, the use of CFD is out of the scope of this project.

3 Methodology

3.1 Design Objectives

The main objective of the cyclone assembly is to continuously separate the solid particles from the gaseous flow of the burner exhaust. The crucial step in the metal fuel cycle is the recycling of the burned fuel (metal powder). In order for the oxidized metal powder to be recycled, it is critical that it is first collected and not thrown out with the rest of the exhaust flow. The cyclone thus needs to collect the metal powder particles at a collection efficiency of 100%. This ensures the highest possible rate of fuel recycling which makes the whole process sustainable and renewable.
Additionally, the exhaust needs to be clean (free of metal particles) so it can be further used for power generation. Hot iron powder in the flow can be damaging to any post-cyclone device. Specifically, a heat exchanger is required to extract heat, and usually the higher the density of the heat exchanger, the higher the extraction rate. Iron particles are abrasive and can clog a particularly dense heat exchanger. This impacts both the efficiency of heat extraction and damages equipment. A secondary objective in relation with the heat extraction step, is that the cyclone needs to retain the most amount of heat possible in the gas flow going to the exhaust. The separation system has to facilitate heat exchange between particles and the gas flow and at the same time have minimal heat loss to its environment.

3.2 Design Parameters

The design parameters of the cyclone are directly related to the characteristics of the turbulent iron burner of the AFL. The first one is the volumetric flow of the burner. The gas flow rate coming from the combustion process is the baseline for the volumetric flow through the cyclone. The combustion flow is determined by the sum of a few different flow components:

- The particle carrier flow
- The primary flow
- The secondary flow
- The tertiary flow

The particle carrier flow is the flow necessary to transport the iron particles from the dispersion system to the burner assembly. Once it reaches the burner's body, it is mixed with the primary

flow. The primary flow rate, directed in the central tube of the burner, carries the powder through the burner and ejects it in the combustion section at the designed velocity and the designed flow rate. The secondary flow is only temporary, it is mixed with the methane to ignite the iron-air mixture. After the iron is ignited, the secondary flow is fully extinguished. Finally the tertiary flow is the one that passes through the swirler of the burner assembly.

The sum of these flow rates is the baseline flow rate that has to be sucked in by the cyclone separator. In addition to the burner flow, the cyclone is designed to aspirate four times that amount air from the immediate environment, the AFL laboratory. The goal is to dilute the burner flow with room temperature flow and thus cool it down. This measure is taken for safety — in the case where combustion of the particles is not complete, re-ignition outside the combustion section is to be avoided. As one of the necessary conditions for ignition and combustion is high temperature, cooling the exhaust flow will avoid ignition, and potentially an explosion, in places that are not designed or monitored for such events. Although the total amount of heat in the flow remains the same, the trade off from this parameter is of course the reduction of temperature of the flow. Additionally, drawing more flow guarantees that the flow coming form the burner will not choke, in case of fluctuations or even a desired burner flow parameter increase. The additional flow helps direct all the powder coming from the burner into the cyclone intake, minimizing powder loss and maximizing collection.

The second major parameter is the solid load of the flow. The dispersion mass flow rate paired with the burner gas flow and the extra air volumetric rate that yields the particle load of the flow entering the cyclone in mass per volume of gas (kg/m^3). The particle load greatly affects the cyclone design and consequently its collection efficiency. The powder mass flow rate is fixed by the power requirements of the burner, since it is the fuel that is being oxidized.

The rest of the design parameters related to the inlet flow of the burner are calculated based on the two primary ones and some material properties. The pressure drop through the cyclone is to be kept to a minimum but it is not a crucial characteristic, given the laboratory equipment available and the fact that this is a proof-of-concept design. It is a parameter to be optimized for future designs.

3.3 Design Constraints

The AFL turbulent iron burner determines the main cyclone design parameters, such as the volumetric flows and particle mass flow rate, as discussed earlier. These design parameters are thus the

primary design constraints of the cyclone, given the cyclone is an addition to the burner system. The cyclone does not affect the burner parameters, since its purpose is only to treat the burner exhaust. The design of the burner is its own complex process. Starting the design with the choice of a cyclone type, the best cyclone format for the project is the slot entry, cylinder-on-cone cyclone. It is optimal for medium to low particle loads, and has a high separation efficiency. It is relatively easy to fabricate, and although the pressure drop should be minimized, it is not the driving design constraint for this iteration of the cyclone.

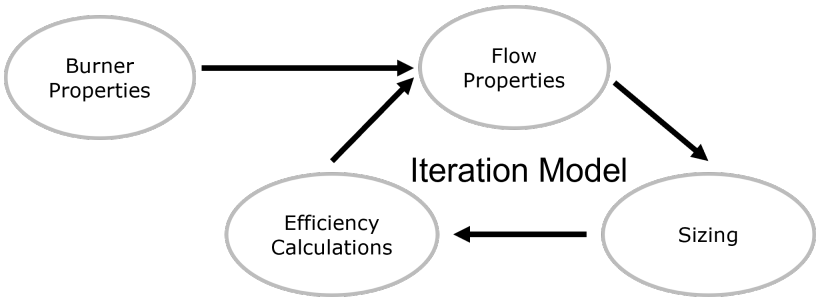

Figure 3.1: Flowchart of the Cyclone Design Process

As discussed, the flow properties influence the physical dimensions of the different parts of the cyclone assembly, but they are not enough to completely define the cyclone design. As shown in Fig. 3.1, the design of the cyclone goes through an iterative process, where the performance of a preliminary cyclone design is evaluated through a numerical model. The volumetric flow rate and particle load, combined with the goal to maximize collection efficiency choices narrow down the sizing possibilities. As a preliminary sizing attempt, the Stairmand high efficiency sizing template is applied, shown in table 3.1. Once the relative sizing between the different dimensions is set, the diameter of the cyclone is to be set. The diameter in its turn gives absolute values to the other dimensions. The dimensions, with the flow properties, are then the input variables for the design iterative model, which calculates the complete parameters of the cyclone, including its collection efficiency and cutoff (x_{50}) diameter. Changes in the dimensions, guided but not necessarily stuck to the sizing template, affect the cutoff diameter, collection efficiency and pressure drop through the cyclone.

The overall physical dimensions also have to be reasonable in terms of space occupation and manufacturing. Since the cyclone is composed of three vertical pieces, the overall height is not manufactured as one. The assembly of different pieces allows for easier manufacture. The tall ceilings and wide spaces in the laboratory room do not constrain the sizing of the cyclone directly. However,

with multiple experiments and experimental equipment present in the room, the management of the space occupation is an important factor. Furthermore it is preferred for the cyclone to be placed as close as possible to the burner exhaust to avoid extra ducting that will impact the flow and possibly the performance. A maximum footprint of $1m^2$ and a maximum height of $2m$ is deemed reasonable for the overall dimensions of the cyclone. This soft constraint can be breached if necessary.

3.4 Iterative Model

This section discusses the compiled model that is used in designing and evaluating the cyclone design. In fact, designing the cyclone is an iterative process that takes a reverse path to a conventional design process. The very first step of the cyclone design is to actually set the geometry of the cyclone.

Table 3.1: Cyclone Designs [29]

Source	Duty	D	a/D	b/D	D_x/D	S/D	$H-H_c/D$	H/D	D_d/D
Stairmand	High Efficiency	1	0.5	0.2	0.5	0.5	1.5	4.0	0.375
Swift	High Efficiency	1	0.44	0.21	0.4	0.5	1.4	3.9	0.4
Lapple	General Purpose	1	0.5	0.25	0.5	0.625	2.0	4.0	0.25
Swift	General Purpose	1	0.5	0.25	0.5	0.6	1.75	3.75	0.4
Stairmand	High Throughput	1	0.75	0.375	0.75	0.875	1.5	4.0	0.375
Swift	High Throughput	1	0.8	0.35	0.75	0.85	1.7	3.7	0.4

As seen in table 3.1, different base geometries are developed for different purposes, and the corresponding variables are shown on the cyclone sketch in Fig. 3.2. A high efficiency cyclone allows for the collection of smaller particles with the trade off of a higher pressure loss through it. A high throughput cyclone on the other hand is more suitable for higher flow processes where less restriction is required. A high efficiency design is chosen for the cyclone, since full collection is required and minimizing the pressure drop is not of a concern at the time. At a further stage, one should aim to minimize the pressure drop, which directly relates to losses, and thus a high pressure drop ends up costing more money to the user of the equipment.

Base Calculations

The first few parameters that are calculated derive from the geometrical properties of the cyclone. The entrance constriction coefficient α derives from the slot entrance duct of the device. It influences the wall velocity $v_{\theta w}$ and the "inner feed" concept, explained later. The empirical formula for the

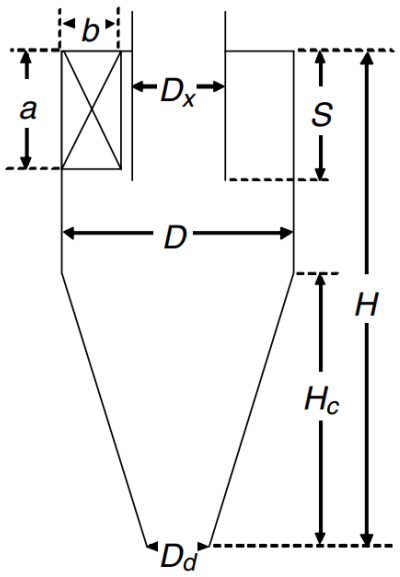

Figure 3.2: Slot Cyclone Dimensions [23]

constriction coefficient is:

$$\alpha = \frac{1}{\xi}\left\{1 - \sqrt{1 + 4\left[\left(\frac{\xi}{2}\right)^2\right]\sqrt{1 - \frac{(1-\xi^2)(2\xi-\xi^2)}{1+c_o}}}\right\} \tag{3.1}$$

where $\xi = b/(1/2D)$ is purely geometrical and c_o is the ratio between the mass of incoming solids to mass of incoming gas. In the AFL system, the feed rate of powder from the dispersion system is known (in $[g/s]$) and so is the volumetric flow rates of the burner, as well as the extra air sucked in from the cyclone (in $[m^3/s]$). Using the density of the gas to find its mass, c_o can be rearranged in $[g_{solids}/g_{gas}]$ or $[kg_s/kg_g]$ for the same unit of time (seconds).

Once the constriction coefficient is found, the wall tangential velocity ($v_{\theta w}$) is calculated. R_{in} is the perpendicular distance from the middle of the inlet ($b/2$) to the centre of the cyclone. v_{in} is simply the inlet flow rate divided by the inlet area ($a \times b$).

$$v_{\theta w} = \frac{v_{in} R_{in}}{\alpha R} \tag{3.2}$$

Next the wall axial velocity (v_{zw}) is calculated. The Trefz and Muschelknautz model approximates that 10% of the inlet flow bypasses the cyclone, thus the 0.9 factor is used. R_m is the geometric mean radius, given by $R_m = \sqrt{R_x R}$

$$v_{zw} = \frac{0.9Q}{\pi(R^2 - R_m^2)} \tag{3.3}$$

Flow Properties

The above calculates velocities are not needed directly in the design of the cyclone, however they are necessary to compute the cyclone's body Reynolds number, which is later necessary. The gas-phase and gas-plus-solids wall friction factors are both a function of the Reynolds number. Once those are obtained, one can calculate the internal spin velocity and the particle cut size x_{50}. These next few steps are presented below. The cyclone body Reynolds number is:

$$Re_R = \frac{R_{in} R_m v_{zw} \rho}{H\mu\,(1 + (v_{zw}/v_{\theta m})^2)} \tag{3.4}$$

where ρ is the gas density, μ is the absolute viscosity and $v_{\theta m}$ is the mean rotational velocity. The latter depends on $v_{\theta w}$, which is already found, and on $v_{\theta CS}$, the inner vortex velocity. However, the vortex velocity is itself dependant on Re_R. Fortunately $(v_{zw}/v_{\theta m})^2$ is much smaller than 1, since the z-velocity component close to the wall is much smaller than the spin velocity close to the wall and this term can then be neglected.

Once the Reynolds number is obtained and the relative wall roughness is set to be 6×10^{-4} for a smooth walled cyclone, the friction factors can be found. The gas friction factor f_{air} is split into two components - one for a smooth wall and one for the wall roughness contribution. Those are empirical values taken from tables, that originally come from the pressure drop theory discussed earlier, and experimental data. The frictional drag contribution of the solids is then added to the gas factor to yield the total friction coefficient:

$$f = f_{air} + 0.25 \left(\frac{R}{R_x}\right)^{-0.625} \sqrt{\frac{\eta c_o Fr_x \rho}{\rho_{str}}} \tag{3.5}$$

The unknown values in eq. (3.5) are the ρ_{str}, Fr and η. The first is the density of the "strand" of particles along the wall. It is obtained by approximating it between 0.3 to 0.5 times the ρ_{bulk}, which is the bulk density of the solids at rest. The bulk density is found by multiplying the density of the material by the packing factor (0.5 for powder). The efficiency of the cyclone, η, is still unknown and has to be assigned a temporary value at the time. The value is above 0.9, since this is the expected and desired cyclone efficiency. It can be iterated a few times once the first efficiency is calculated. Finally the Froude number Fr, which is a ratio of flow inertia to external factors, is

given by an equation dependant on the axial velocity through the inlet section and gravity (external force).

Cyclone Performance Properties

With the total friction factor calculated, the inner vortex velocity $v_{\theta CS}$ can be found by eq. (3.6), where A_R is total inside area of the cyclone contributing to frictional drag (i.e. the total inside area without the collection bin). Finally, knowing $v_{\theta CS}$ allows us to calculate the much needed cutoff diameter of the cyclone, x_{50}, with eq. (3.7). It is interesting to note that eq. (3.7) is closely related to eq. (2.6), which is the ratio of the particle velocity to a critical velocity, determining if the particle gets separated from the flow. As discussed in section 2.2, that equation then relates to the critical diameter, d_{50}, also called x_{50}, as seen here below. These two equations have in fact the same variables, but eq. (3.7) is slightly corrected from empirical data.

$$v_{\theta CS} = v_{\theta w} \frac{(R/R_x)}{\left[1 + \frac{f A_R v_{\theta w} \sqrt{R/R_x}}{2Q}\right]} \tag{3.6}$$

$$x_{50} = \sqrt{\frac{18\mu(0.9Q)}{2\pi(\rho_p - \rho)v_{\theta CS}^2(H - S)}} \tag{3.7}$$

It can be seen directly from eq. (3.7) that the longer the cyclone (H), the smaller the cutoff diameter is. A lower gas flow, Q, increases the particle load and decreases the cutoff diameter, since the there is less carrying flow. This in fact brings the discussion of mass loading effect, or saltation, occurrence. This phenomenon occurs when the mass fraction of the incoming solid particles exceeds the limit-loading of the gas flow. This limit is the amount of solids that the turbulent flow inside the cyclone can hold in suspension. In the case that it is exceeded, a fraction of the entering particles are immediately centrifuged to the walls of the cyclone, where they proceed to fall down and get collected. The rest of the particles undergo the usual separation process within the inner vortex. In fact, when mass loading effect occurs, the cyclone becomes a sort of a two-stage separator. As for the inner vortex separation, the very simple eq. (3.8) gives the separation efficiency for a given particle size, x_i. The factor m represents the slope of the cutoff curve and it is an empirical value between 2 and 7. For a smooth walled cyclone that operates under design conditions, the value 5 is chosen as appropriate.

$$\eta_i = \frac{1}{1 + \left(\frac{x_{50}}{x_i}\right)^m} \tag{3.8}$$

The individual separation efficiency elements are then summed up over the range of the particle distribution. The distribution is usually given in discrete steps of diameter and their respective weight fractions, ΔMF_i, from 1 to N.

$$\eta = \sum_{i=1}^{N} \eta_i \times \Delta MF_i \tag{3.9}$$

In the case that mass loading occurs, the individual efficiency equation, eq. (3.8), remains the same. What changes is the mass fraction which gets separated by the inner vortex method and the one by limit loading. Thus the total efficiency formula becomes:

$$\eta = \left(1 - \frac{c_{oL}}{c_o}\right) + \left(\frac{c_{oL}}{c_o}\right) \sum_{i=1}^{N} \eta_i \times \Delta MF_i \tag{3.10}$$

The fraction $\frac{c_{oL}}{c_o}$ is the part that experiences inner vortex separation. Consequently, $1 - \frac{c_{oL}}{c_o}$ is the mass fraction that gets separated by the mass loading occurrence. The inlet loading c_o is known by this point, and it is compared to the limit loading c_{oL}. The latter is found with an empirical formula that takes the ratio of the cutoff diameter to the median diameter of the particle distribution and multiplies it by the mass loading ratio risen to a factor of a value below 1.

This process, shown here in a simplified version, concludes the first iteration of the cyclone design process. As seen, some values need to be updated after the first iteration and the calculations need to be ran multiple times to narrow the design to the desired output. To facilitate that process, all the necessary equations, variables, inputs and outputs are combined in an Excel spreadsheet. The spreadsheet also makes use of macro functions to iterate over parameters and optimize the design.

An important part of the design is choosing the driving device for the flow. The gas-solids flow can be pushed in, or pulled out of a cyclone. In terms of this project, it means that the burner flow is to be pushed with a blower upstream of the cyclone, or pulled with a fan downstream of the cyclone. Since the design of the system is to be an open system, the latter choice is preferred. If a blower is chosen to push the flow, this would result in a positive pressure differential inside the cyclone compared to the surroundings. The system would thus be pressurized. Instead, a fan pulling the flow through the cyclone results in a negative pressure differential between the the cyclone and surroundings, making the system slightly vacuumed.

The pressure drop through the cyclone is then a necessary property to design the overall system. It dictates the sizing of the fan that is pulling the flow through a cyclonic separator, or any ducting system in fact. The calculations for the pressure drop are not shown in detail. In fact, the pressure drop is calculated simply to verify that the existing fans in the lab are powerful enough to be purposed as the pulling fans of the cyclone. The pressure drop through the cyclone is minimal, less than 20Pa.

Final Properties and Characteristics

Before proceeding with design iterations, the Excel model is verified with two worked out example problems from Hoffman's *Gas Cyclones and Swirl Tubes*. After small adjustments of variables and formulas, the model obtains the same results as the examples given by Hoffman. The first step is then to run the model with the known variables and initial sizing dimensions. The known variables, some of which are shown in table 3.2, are the flow and solids properties.

Table 3.2: Key Cyclone Properties

Gas Flow Rate $[CFM]$	Particle Load $[g/m^3]$	c_o	c_{oL}	x_{50} $[\mu m]$	Collection Efficiency η	Pressure Drop [Pa]	Cyclone Reynolds
28	187.5	0.354	0.062	5.91	0.935	19.43	61.75

The initial sizing template chosen is the Stairmand High Efficiency shown in table 3.1. However, after a few iterations, the template used is changed to the Swift High Efficiency one. The Swift design yields a higher efficiency for the working conditions, which is the main goal of the cyclone prototype. The final dimensions for the cyclone separator that are yielded from the iterative design model are shown in table 3.3.

Table 3.3: Cyclone Design Dimensions in $[mm]$

D	a	b	D_x	S	$H - H_c$	H	H_c
200	88	42	80	100	280	780	500

A crucial input parameter for calculating an accurate cyclone performance from the model is the particle size distribution. Although the cutoff x_{50} diameter of the cyclone does not depend on the solid particles distribution, the collection performance does depend on it. In fact, depending on the particle distribution, the relevant range of the GEC will change. For example, if the particles

distribution spans from $0.2\mu m$ to $100\mu m$, the full range of the predicted GEC will be utilized, as shown in Fig. 3.3. However if all particles are larger than $10\mu m$, only the right-side tail of the GEC is relevant.

An important observation to note in Fig. 3.3 is the the fact that there are two GEC curves, one considering the entrance separation effect and one that does not. Referring to the discussion surrounding eq. (3.10), entrance separation occurs when the particle loading c_o introduced in the cyclone exceeds the limit loading c_{oL}. The cyclone then effectively has two separation zones, the entrance and the inner vortex. Two phenomena arise from this effect, which both improve the collection efficiency. Firstly, smaller particles get entrained by the larger particles that are immediately separated at the cyclone entrance, which increases the cyclone performance in the lower particle size range. Secondly, once in the inner vortex, the flow velocity is faster than what it would be without entrance separation and thus the cutoff diameter of the cyclone is reduced, again improving its performance [23, 19]. This effect however is not observed for very high $\frac{c_o}{c_o L}$ ratios.

This first iteration of the cyclone is expected to run at a loading ratio of 1.13. Although it might seem very close to a ratio of 1, it is high enough to increase the cyclone efficiency, particularly for particles below the cutoff diameter x_{50}. As shown in Fig. 3.3, the red curve (which considers limit loading) is higher on the left side of $10\mu m$. For particles larger than 10 microns, the efficiency remains the same both in the case of limit loading or not.

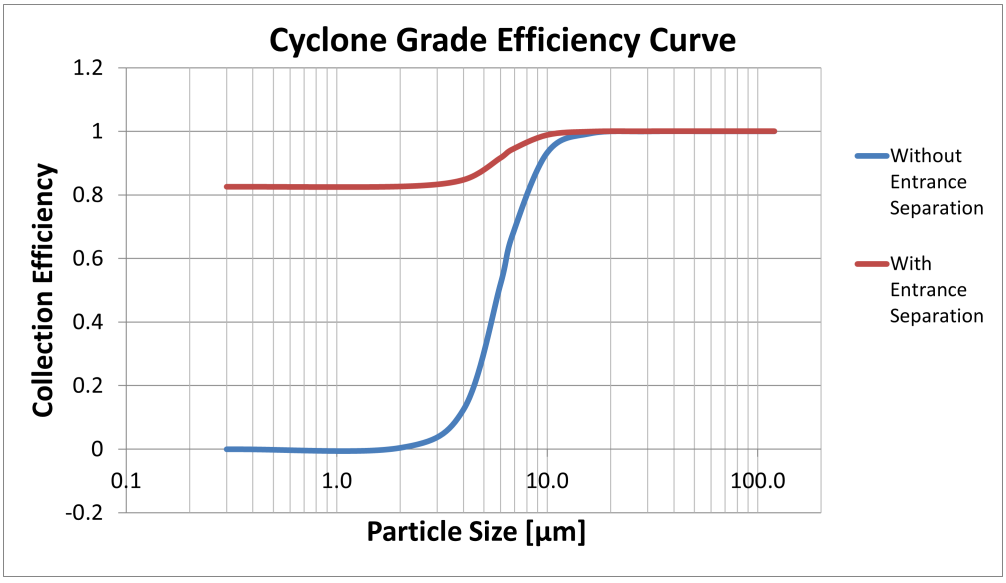

Figure 3.3: Predicted Grade-Efficiency Curve for the Designed Cyclone

The first iteration of the design is calculated with an approximation of the powder size distribution.

The powder size distribution is taken from a powder batch previously used for experiments by the Alternative Fuels Lab. As shown in table 3.2, based on the particle size distribution assumed, the predicted overall efficiency of the cyclone is 93.5%. Although the overall efficiency is not 100%, it is deemed high enough as a first iteration. There are a few different reasons for that decision. Firstly, as it can be seen in Fig. 2.1, cyclones are not recommended to be used for particle sizes of less than $2\mu m$. The cutoff diameter of about $5\mu m$ is thus at the lower limit of the recommended solids input for a cyclone. The second reason is that the powder used for the turbulent burner is expected to have a larger size distribution than the one that was previously used by the AFL. The previous experiments in fact require smaller particles to facilitate particle suspension; the burner used for those experiments is not a high-flow self-sustained turbulent burner and cannot keep heavy particles suspended long enough for combustion. Finally, if the actual collection efficiency is below what is expected, flow parameter can be adjusted and geometry and fabrication can be iterated to increase the collection rate. It is important to note however that following the predicted cutoff diameter and steepness of the GEC curve, particles of size $10\mu m$ have expected separation efficiency of 93%. The rate exceeds 99% for particles of a diameter larger than 16 microns.

4 Manufacturing

4.1 Manufacturing Constraints

The first constraint for the manufacturing of the cyclone separator are of course the physical dimensions. The inner diameter of the cyclone is 200mm and its height is 780mm, excluding the collection bin. The cyclone is composed of a cylinder top piece, which also has to accommodate for the inlet and outlet of the cyclone. Under the cylinder is the conical piece, which leads to the collection bin. The cylinder has a diameter of 200mm and is 280mm high, and the cone diameter goes from 200mm to 80mm in a height of 500mm. The inlet of the cyclone is a rectangular opening on the side of the cylinder section, 12.52mm from the top and 12.52mm from the side. The opening itself is 42mm by 88mm. The two other main parts of the cyclone are the top cap where the outlet is, and the bottom collection bin. The cap is a 200mm disk with a lip and a centered circular opening, in which the outlet tube is installed. The collection bin is a 80mm diameter, 152mm high cylinder closed on one end.

The second constraints for the cyclone is the necessity for air tightness of the assembly. Although the system is considered an open system (not pressurized), there is a small negative pressure differential inside the cyclone, on the order of 20Pa. The negative pressure differential directs the flow from the inlet to the outlet of the cyclone. Air tightness is necessary to maintain the pressure differential, avoid leaks and direct the flow in the right path.

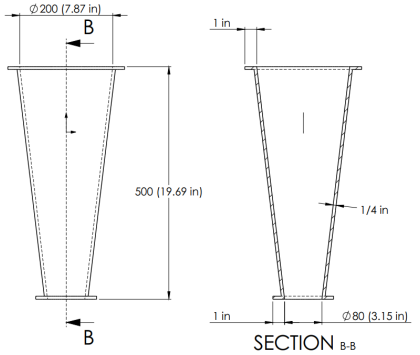

Figure 4.1: Drawings of the First Iteration of the Cyclone Cone

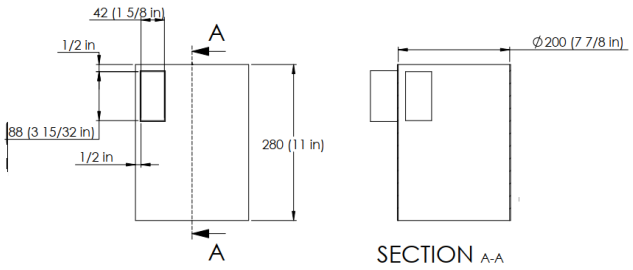

Figure 4.2: Drawings of the First Iteration of the Cyclone Cylinder

The material from which the cycle is produced has to be heat resistant. Although the flow during testing and operation is initially designed to remain under 500°C, the assembly material is chosen to withstand higher temperature. This is to eliminate the possibility of equipment failure in the event

of a malfunction or unforeseen circumstances. Furthermore, it is expected in the future to conduct experiments with higher temperature flows, as part of the secondary objectives of the projects, heat extraction from the burner-cyclone system and a second iteration hot cyclone design. The inside surfaces of the cyclone must be smooth, to avoid disturbances of the flow and to avoid sintering of hot particles. For these reasons, the cyclone is at first designed to be manufactured from machined stainless steel. Stainless steel is corrosive resistant, heat resistant and can be machined to a smooth finish. Although it is more difficult to machine than carbon steel because of its hardness, that makes it more durable and stronger too.

In terms of secondary characteristics, the cyclone has to have the ability to be assembled and disassembled with ease. Since this design is the first of its kind and modifications are expected, the assembly must have the largest amount of separate parts, without increasing manufacturing complexity. The advantage of having the ability of easy assembly allows for parts swap if the user desires to try out different configurations, or in case a part becomes problematic. The collection bin at the bottom of the cyclone has to be particularly easy to install and remove, in order to allow for easy, quick and periodic powder retrieval. The assembly must also include junctions between the different parts that will not impede the flow or create unwanted flow disturbances, such as turbulence.

The cyclone assembly also needs an inlet and an outlet adapters to connect it to the laboratory ducting system, as well as standard metal ducting.

Finally the assembly must be able to support its own weight, keep its form, and be subject to some reasonable external forces (handling, attaching it to a frame, etc).

4.2 Fabrication

To accommodate all the constraints, the first design of the cyclone assembly is considered with flange connections between the vertical parts. The cap, cylinder, cone and bin are all designed to be connected with 25.4mm flanges between them. Flanges are connections that allow for excellent air tightness with the help of a gasket or an o-ring, and are easy to assemble and disassemble. Furthermore, flanges allow for relatively large dimension tolerances, making manufacturing and assembly and handling easier. The cyclone is also designed to be manufactured from 304 stainless steel, with relatively thick walls (1/4”). This allows for high heat resistance as well as resistance to abrasion. The CAD drawing of the assembly is shown in Fig. 4.3, and the cone and cyclone are shown in Fig. 4.1 and Fig. 4.2 respectively.

A lathe is the most commonly used tool to produce circular parts from stock material, and the one available at the McGill Machine Shop. All the parts of the body of the cyclone are circular, thus they need to be turned on a lathe. As for the rectangular opening on the top cylinder, an end mill is necessary. Welding is used to to attach the inlet and outlet of the cyclone.

After discussion with the machinists team at McGill University about the design and its manufacture, a challenge rises with the fabrication of the conical piece of the cyclone. The tool necessary to create the sloped wall cannot reach in through the whole piece. In other words, the 500mm dimension of the cone is too large to be produced at the McGill equipment.

To respond to the fabrication issues, the design of the cyclone assembly is changed slightly, with a different manufacturing method in mind. Using subtractive manufacturing from a large stock piece that can accommodate the overall dimensions of a given piece is costly, time-consuming, wasteful and requires specific tools. Instead, the hollowness and the relatively regular shapes of the cyclone (cones and cylinders) are used as a way of simplifying the manufacture. Similar to HVAC ducting, the main parts of the cyclone can be made out of sheet metal. Sheet metal shaping does not require specific tooling, only mostly cutters, benders and rollers. Tack welding is used to hold the bends together and to attach the external outlet and inlet parts. The drawback from using sheet metal is the reduction in wall thickness - in order to successfully bend the metal into shape, its thickness is significantly smaller than the originally designed wall thickness of the cyclone. This leads to lower thermal resistance, which will lead to higher heat loss towards the outside. Additionally, the thin walls might get too hot through their thickness due to the lower heat dissipation in the material (since there is less material), which might compromise their

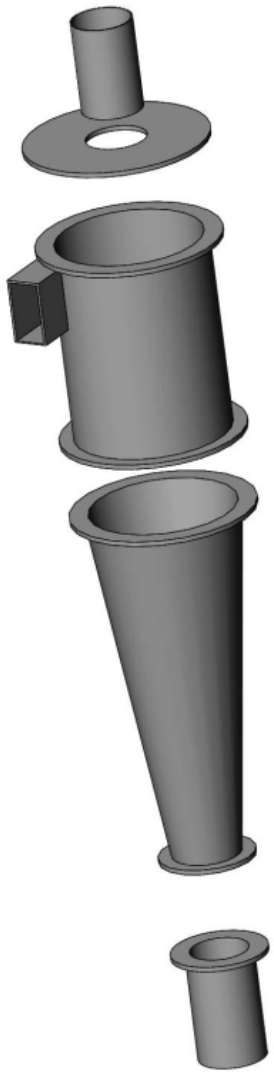

Figure 4.3: First Iteration of Cyclone Manufacture Drawings

structural properties. However it is considered that due to the temperature management technique of hot flow dilution, the cyclone walls will be maintained at temperatures lower than critical. Additionally, the sheet metal cyclone connection points between the different parts are not as seamless as a flanged design since the pieces are stacked one into another. However due to the fact that the seams will be air tight and given the high flow rate of the system, this is deemed insignificant.

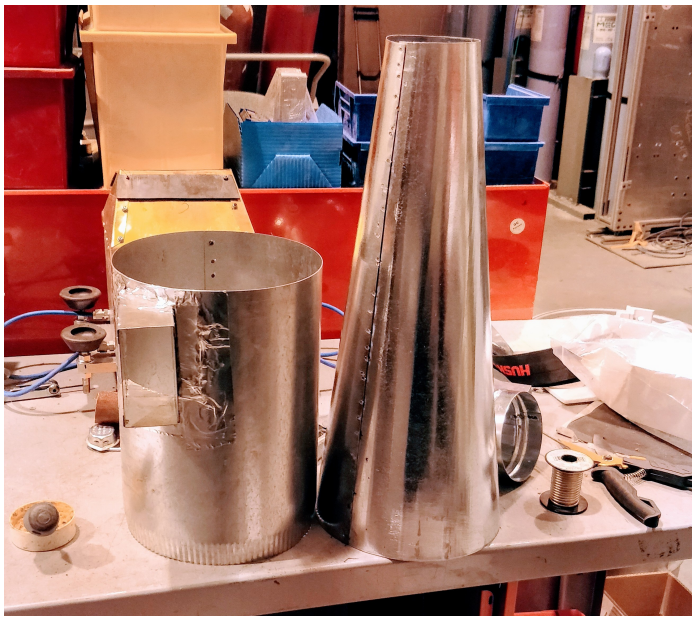

Figure 4.4: Cyclone Parts Manufactured Out of Sheet Metal

Sheet metal makes the design much lighter, easier to install and easier to manipulate. Changes are also easier to make, due to the simpler handling and lack of need for special tooling, increasing the design's versatility. The significant decrease in cost, lead time and complexity further confirms the sheet metal concept as the design of choice.

Since the machinists at McGill University do not have experience with sheet metal bending, the fabrication is outsourced. Due to its resemblance to HVAC ducting, the cyclone design is produced by a custom ducting company in Montreal. The company, Metal Action, has experience in working with custom projects and uses galvanized steel for most ducting projects. The thickness of the cyclone is determined by the capability of Metal Action to bend the metal sheets into the required shape and it is 20 gauge (0.911 mm). The two vertical pieces - the cylinder and the cone - mate together by inserting one in the other. The cylinder's diameter is slightly reduced by having a crimped band of about 25mm. This 25mm-band enters the top of the cone, and the two are screwed one to another for rigidity. Aluminum tape is then used to seal the gaps. This method

is used to attach all the parts of the cyclone, except for the collection bin because it needs to be retrieved often. The bin is hanging from the the bottom of the cone with the help of hinges, and the gap is also sealed with aluminum tape.

5 Experimental Setup

5.1 Lab Setup

The cyclone collection system's purpose is to separate the solid particles from the burner's exhaust flow, resulting in particle collection and a particle-free exhaust. The cyclone inlet duct is connected just after the outlet of the combustion chamber, with a small air gap in between. This air gap allows for ambient air to get drawn by the cyclone, such that the additional air flow to the burner flow that the cyclone is pulling in does not disturb (pull on) the burner flow. The exhaust flow is fed into the cyclone which separates the particles from the gas and discards the fluid. Since the laboratory space already has a cyclone-filter system used for filtering the exhaust of other experiments, this device is used for the newly designed cyclone as well. The existing system is much larger, both in terms of size and flow rate and it is connected to multiple experiments. Connecting the new cyclone to the existing system ensures that the flow exhausted to the surroundings is clean and harmless. Furthermore, it serves as a pulling force for the flow through for the new cyclone. Because the speed of the fan cannot be adjusted, and consequently neither its flow rate, a "Y" duct split to the surroundings is installed downstream of the new cyclone. The damper on this split determines what fraction of air is drawn directly from the surroundings, bypassing the cyclone, and what fraction is drawn from the cyclone itself. Adjusting the opening of the damper adjusts the right flow rate through the cyclone, as depicted in Fig. 5.1. It can be seen that just upstream of the damper, a pleated high-efficiency filter is installed. Its purpose is to catch any particles that escape the cyclone. The red "X" denotes the collection bin of the newly designed cyclone. The blue arrows show the openings through which the cyclone will intake the extra surrounding air, added to the exhaust flow.

For safety concerns, the burner assembly is placed in a clear acrylic enclosure. Consequently this results in the cyclone having to be placed about $2m$ away from the burner. Since the burner is vertical and its exhaust is upwards, a 90°elbow and a horizontal section of rigid ducting is necessary to direct the flow to the cyclone. The cyclone is placed at a height so that the ducting does not go downward, it rises vertically upwards and then remains horizontal. This is to avoid particle accumulation in the ducting. The cyclone is mounted on a frame of extruded "80/20" t-slot aluminum. The collection bin is at a comfortable height for retrieval and empty. This setup can be seen in Fig. 5.2 and Fig. 5.3.

The damper opening downstream of the cyclone is adjusted to achieve the specification flow rate

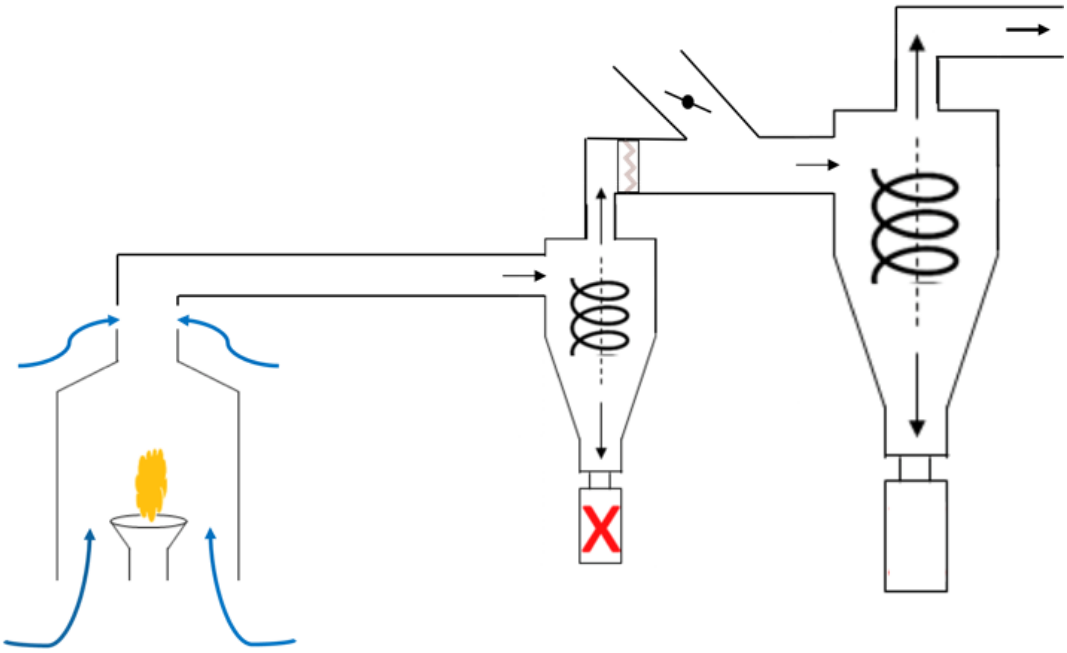

Figure 5.1: Sketch of the Experimental Setup

through the cyclone. The method of adjusting the flow rate is by measuring the flow velocity at the entrance of the cyclone ducting. The velocity is measured with a digital anemometer. Knowing the duct area, the flow rate is then calculated and adjusted accordingly.

5.2 Testing Procedures

Because the cyclone's main task, the primary testing procedure for the cyclone is targeted towards evaluating the separation efficiency. Testing the cyclone is a multiple step process and the first crucial step is to measure the quantity of solids that enter the cyclone.

This proves to be a difficult task, at least to a high accuracy. Dispersing and suspending solid particles in a gas flow is in fact the main challenge the turbulent burner is trying to overcome. The dispersion system used to disperse the iron powder into the burner-cyclone is a custom system from *Powder & Surface GMBH*. The dispersion system has a powder bin where the solid iron is loaded. The system then sucks in powder in two chambers, alternating them, in order to avoid peaks of powder dispersion. The powder from the chambers is then expelled in a tube that is connected to the desired equipment, in this case the burner. Multiple parameters can be adjusted, such as the vacuum strength and the powder feed gas pressure. These affect the amount of powder fed into

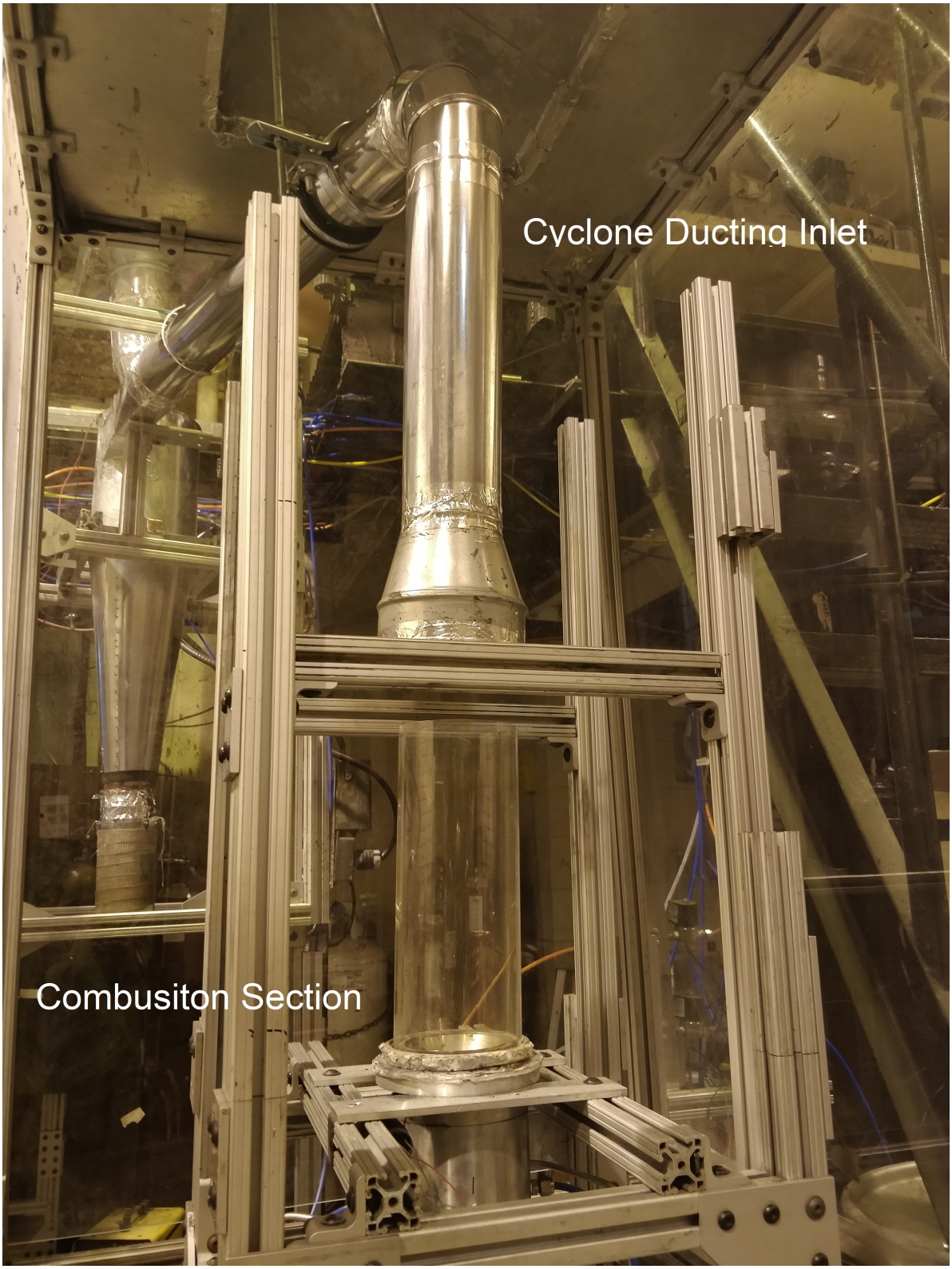

Figure 5.2: Burner Combustion Tube with Cyclone Ducting and Cyclone in the Back

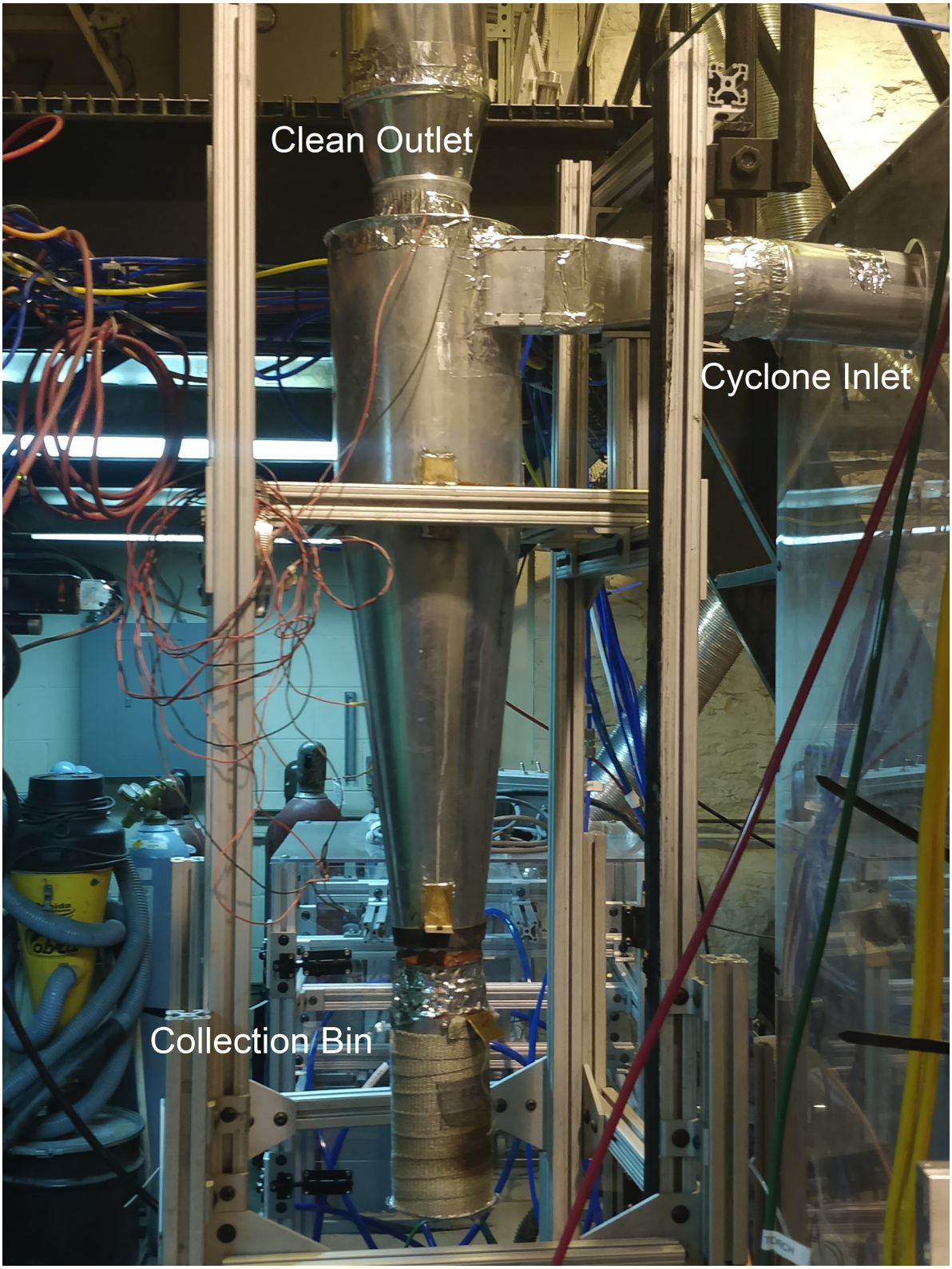

Figure 5.3: Cyclone Separator mount

the chambers and the pushing strength out of the chambers respectively. Although the dispersion system is of top quality and sticks to the set parameters within a small tolerance, the powder mass flow rate is visibly inconstant. This is due to the heavy, dense iron powder and the difficulty in overcoming gravity and friction. The dispersion system is calibrated by doing dry runs: the main feed tube is disconnected from the last connection before the burner, and is instead inserted in a closed container. The dispersion is ran for a certain amount of time, and the mass of the powder dispersed in this time is recorded. The mass dispersed averaged by the dispersion time yields the mass flow of the powder in [g/s].

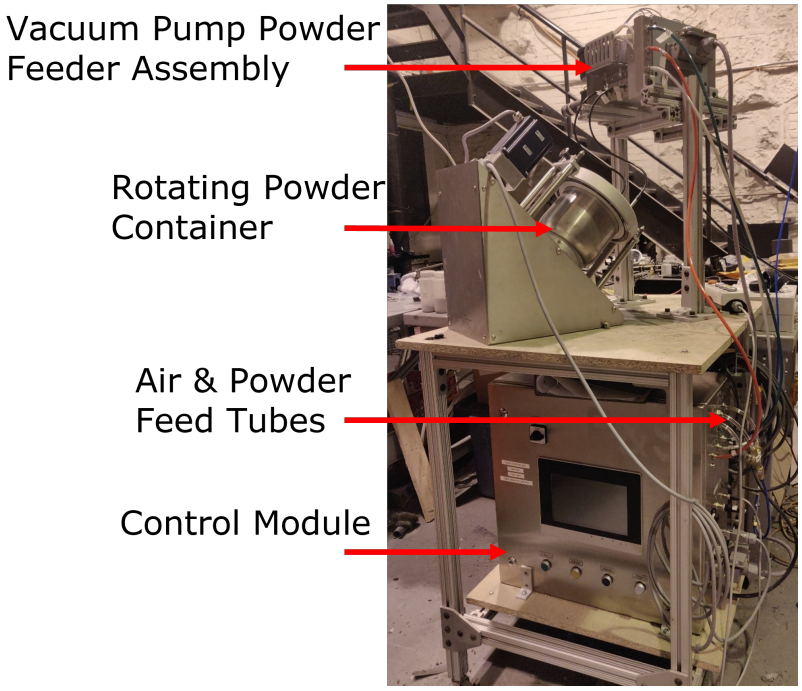

Figure 5.4: Dispersion System Coupled to the Burner-Cyclone Experiment

The next step is to adjust the gas flow that the cyclone draws. Closing or opening the damper downstream of the cyclone, shown in Fig. 5.1, directs more or less flow through the cyclone separator. The flow velocity is measured with a digital anemometer and the volumetric flow rate is calculated (by knowing the duct cross-sectional area). The damper is adjusted to achieve the desired flow rate.

The burner is then operated with powder dispersed through it. The powder has to be dispersed through the burner in order to achieve a somewhat even dispersion in the form of a cloud. If the powder is fed in the inlet ducting straight from the supply tube, it comes out as a jet rather than a cloud of particles.

The testing procedure itself is quite simple. It begins with the exhaust filter's mass being measured and recorded before the powder is dispersed. The cyclone collection bin is also emptied and weighed, with its mass is recorded. They are both reinstalled in place and sealed for air tightness. After having calibrated the dispersion and adjusted the cyclone inlet flow, the cyclone fan is turned on. A timer is started at the same time as the dispersion is triggered into the burner. The powder line is primed from previous runs. The timer is stopped when dispersion is halted, and the time is recorded. With the dispersion time known, the quantity of dispersed powder is calculated by multiplying the time of dispersion to the rate of dispersion. Once the cyclone fan is stopped, the collection bin is removed and weighed as is, with the powder inside. Carefully, the filter is also weighed. If particles escape the cyclone, they are stopped and collected in the filter. The mass difference of those two components from before and after the dispersion is calculated and recorded. The interpretation of the measured data is discussed in section 6.2.

Figure 5.5: Self-sustained Turbulent Iron Burner Flame

6 Results & Discussion

6.1 Particle Sizing

The first property examined is the powder size that is to be used in the system. It is important to know particle properties before and after the powder has been through the process, in order to understand and evaluate the oxidation process and collection mechanism. It is expected that the iron powder is to gain in volume and weight after being burned.

Combustion is, simply put, very rapid oxidation. Although iron combustion and oxidation will not be discussed in detail since it is not part of the project objectives, it is briefly discussed to give background to the results and analysis. When combusted, or oxidized, pure iron particles react with oxygen to produce iron oxide. There are different forms of iron oxide that form under different oxidation conditions. At the time, it is still unclear which form, or combination of forms, is to be observed at the end of the combustion process in the AFL burner. More details are discovered about the oxides and oxidation processes with the help of Scanning Electron Microscope (SEM), Thermogravimetric Analysis (TGA) and X-ray Diffraction (XRD) experiments, discussed in section 6.3, section 6.4 and section 6.5 respectively. It is known for now that as pure iron (Fe) oxides, or combusts, it gains in oxygen molecules to produce iron oxides. As discussed in section 1.1, combustion of iron particles leads to larger and heavier solid iron oxide particles.

To obtain a profile of the powder size distribution, batches of the experimental iron powder are analyzed by the McGill Materials Characterization Lab. The sizing of the powder sample is performed with a Horiba LA-920 particle size analyzer. It is a laser diffraction, implying that laser light that is shined on examined particles is diffracted by them and captured by a sensor. This method is quick, reliable and reproducible [41].

Two samples of powders are subjected to the laser diffraction technique: pure iron powder to be used for the experiment, prior to being subjected to any process, and powder that has undergone combustion in the turbulent burner and cyclone collection. The latter is extracted from the cyclone powder collection bin, as shown in Fig. 6.4. The powder is dispersed in the burner, burnt in the combustion cylinder, from where it enters the cyclone inlet duct and is separated from the gaseous exhaust inside the cyclone. At this point the efficiency of the cyclone is not yet evaluated, but it is known that the powder collected in the bin has undergone combustion. Three different batches of powder are analyzed, all of them very similar in initial sizing.

It can be seen in Fig. 6.1 that in all three cases the burnt (collected) powder has a wider distribution

Table 6.1: Particle Sizing Analysis on Burnt and Unburnt Powder Samples [μm]

Sample	D10	D50	D90	Mode	Mean	Median
Unburnt 1	10.45	17.49	26.69	18.66	18.20	17.49
Burnt 1	12.00	21.32	37.28	21.39	23.82	21.32
Unburnt 2	10.21	16.42	24.73	18.49	17.02	16.41
Burnt 2	13.11	24.71	53.86	24.27	30.36	24.71
Unburnt 3	10.59	17.33	25.71	18.65	17.84	17.33
Burnt 3	12.42	24.07	62.96	21.35	32.86	24.07

than the unburnt powder, and its peak is shifted to the right. The wider distribution can be explained by two factors: the uneven gain in volume of particles and sintering of particles together. As it is still unknown to what extent the combustion is completed, different particles are most probably subject to different forms and levels of oxidation. Secondly, some particles stick together by a sintering mechanism.

Combustion of the powder results in at least a partial melt of particles, which in turns result in particles sticking to one another when in contact. The large tail of the burnt particles curve is another evidence for sintering. In the unburnt powder analysis, no particles are bigger than roughly $50\mu m$. However in the analysis of the burnt powder, particle size reaches the hundreds of microns, up to 4 times larger than the largest initial size of the iron particles. As discussed in section 1, iron particles do gain oxygen molecules in the combustion process, resulting in larger particles. However, even if the largest possible oxides are formed, they would not be 4 times larger than the pure iron powder size. The Pilling-Bedworth ratio is the volume ratio of the volume of metal oxides to the volume of the corresponding metal, and it is used to evaluate the volume gain of an oxide state. If it is considered that all the particles completely oxidize to Hematite (Fe_2O_3), the Pilling-Bedworth ratio for Hematite to iron is of 2.1. The ratio for Wustite to iron is 1.7 and Magnetite to iron, 1.9. The large increase of the collected powder by 4 times the initial volume of the iron particles is thus not explained by the oxide formation, but rather particle sintering.

Two important observations are made with respect to the cyclone separation efficiency. Firstly, as per the sizing analysis, no sample of the unburnt powder contains particles of less than $4\mu m$. Additionally, less than 1% of the particles are sized below $6\mu m$. Considering the design cutoff diameter of the cyclone which is $5.91\mu m$, the cyclone separator should collect at least 99% of the particles (assuming the whole 1% below 6 microns is lost). Furthermore, as particles increase their size in the process of combustion, the detailed sizing data from the burnt samples shows that

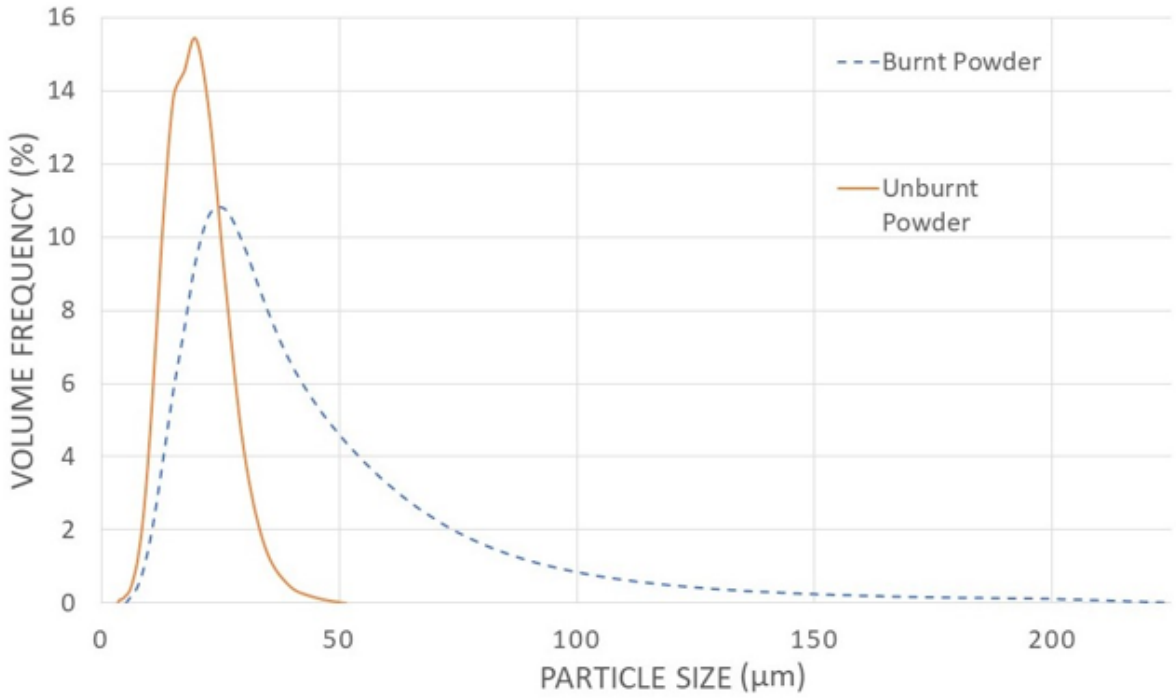

Figure 6.1: Particle Size Distribution of Unburnt and Burnt Powder

approximately only 0.3% of them are below $6\mu m$. The cyclone separator is then expected to achieve and surpass the predicted efficiency from the model, given the iron powder used in this experiment.

6.2 Collection Efficiency

Once the cyclone separator is built and commissioned, its performance needs to be evaluated. Given the setup of the collection system, it is assumed with confidence that particles cannot escape to the surroundings. The filter installed right downstream of the cyclone stops any solids that escape the cyclone. Thus particles that are dispersed can end up in three possible locations – they do not enter the cyclone duct at all, they end up in the cyclone or its ducting, or they are captured by the filter after escaping the cyclone. Although it is assumed that any particle remaining in the cyclone or its ducting is collected, visual inspection shows there is no accumulation of iron powder in the ducting or cyclone walls. Once powder enters the separator ducting, it is either collected in the bin, or escapes to the filter.

The particles that are to be collected by the cyclone have to be dispersed through the burner. The burner achieves a fairly even spatial distribution of the particles, prior to them entering the cyclone inlet ducting. If the particles do not go through the burner, i.e. they come out of the dispersion system tube directly, they are bunched up in a small diameter stream and a good spatial distribution

in the cyclone ducting is not achieved. This leads to particles falling right down vertically, and not being entrained in the cyclone flow. Furthermore, the burner has to be producing a flame in order to carry the particles vertically to the cyclone duct. If the run is "dry", i.e. with no flame, particles cannot travel long enough to reach the cyclone ducting and once again, fall back down.

A GoPro camera is setup inside the cyclone to examine the particle collection process as it is happening. As shown in Fig. 6.2, the camera is setup on the bottom of the conical section, looking upwards towards the inlet and outlet of the cyclone. Figure 6.3 shows a snapshot of the camera footage. The circular dark black lines are in fact iron powder spiraling down towards the camera. It is clear from the video that the flow of the particles is as modelled and predicted and that particles do not stick to the cyclone walls. The latter is also observed upon opening and inspecting the inside of the cyclone.

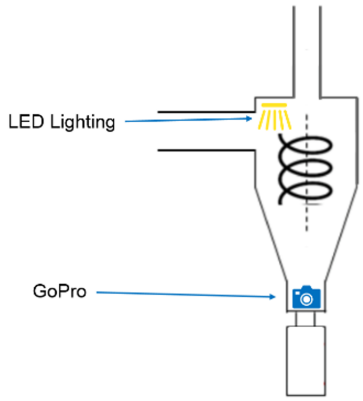

Figure 6.2: Sketch of the GoPro Camera Setup Inside the Cyclone

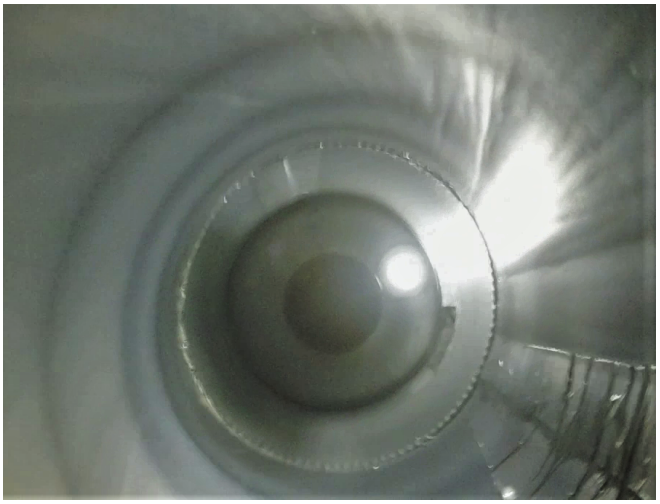

Figure 6.3: Snapshot of the GoPro Recording

The first and most important uncertainty in this efficiency experiment is knowing the quantity of dispersed powder in the burner. As explained, although the dispersion system is calibrated and maintains the set parameters to a high accuracy, the physical properties of the iron powder make it difficult to achieve a uniform dispersion throughout the time of the experiment. Additionally, the overall dispersion rate cannot be measured in real time.

It has to be taken into account that when undergoing oxidation, the iron particles become iron oxides and gain in mass. The most common states of iron oxide are wustite, magnetite and hematite. They are denoted by FeO, Fe_3O_4 and Fe_2O_3 respectively. The stoichiometric oxidation reactions leading to them are given below. Although the oxygen molecules come from the supplied air, the interest is in the solid products and the reactions shown are isolated for the oxidation process only without

Figure 6.4: Powder Collected in the Cyclone Bin

taking Nitrogen and other elements into account. When mass analysis is done on the oxidation reaction equations, the mass increase rate of the iron transforming into an oxide is found. The results of that calculation is shown in table 6.2. If iron particles from a batch oxidize completely to magnetite, the weight of the solid products increases by a ratio of 1.38 to the solid reactants.

$$\mathrm{Fe\,(s)} + \tfrac{1}{2}\mathrm{O_2\,(g)} \longrightarrow \mathrm{FeO\,(s)}$$
$$\mathrm{Fe\,(s)} + \tfrac{2}{3}\mathrm{O_2\,(g)} \longrightarrow \tfrac{1}{3}\mathrm{Fe_3O_4\,(s)}$$
$$\mathrm{Fe\,(s)} + \tfrac{3}{4}\mathrm{O_2\,(g)} \longrightarrow \tfrac{1}{2}\mathrm{Fe_2O_3\,(s)}$$

Table 6.2: Particle Sizing Analysis on Burnt and Unburnt Powder Samples [μm]

Oxide	Reactant (Fe) Molar Mass (g)	Product Molar Mass (g)	Mass Ratio
Wustite FeO	55.85	71.84	1.29
Magnetite Fe_3O_4	55.85	77.18	1.38
Hematite Fe_2O_3	55.85	79.85	1.43

Given that FeO is unstable at ambient conditions, it is believed that the oxides collected cannot be wustite. Additionally, the color of the oxides as seen in Fig. 6.4 are dark-grey, black. The color of hematite is rather red-orange, rust color. For this reason, it is believe that the collected oxides are not hematite, but are rather magnetite, Fe_3O_4. The exact composition of the collected powder

is further discussed in sections 6.3 to 6.5.

The other factor determining the mass gain of the combustion products is the level of combustion, the composition of the collected dust. If all dispersed iron undergoes complete combustion, it is expected that the products are 100% Fe_3O_4. However, incomplete combustion leads to a combination of iron and iron oxide in the collection bin of the cyclone. Consequently, the mass increase of the separated powder with respect to the initially dispersed quantity of iron is expected to be of a ration between 1 and 1.38. Visually, practically all the collected powder is of darker grey than the fresh iron, meaning it has reacted, at least partially. This color difference is seen in Fig. 6.5.

Figure 6.5: Powder Sample Collected on the Left Compared to Pure Iron Powder on the Right

Table 6.3: Collected Iron Powder Mass During Experiments

Running Time (s)	Mass Dispersed (g)	Mass Collected (g)	Mass Ratio	Mass Gain by Filter (g)
351	368	471	1.28	0.1
279	312	349	1.12	0.0
242	271	336	1.24	0.0
348	400	504	1.26	0.1
371	426	550	1.29	0.0

The results seen in table 6.3 are expected and within the predicted range. The conclusion that can be drawn from the data is that no particles escape the cyclonic separator. Since the filter has not gained any mass throughout all the experiments, it can be concluded that no particles are present in the outlet of the cyclone. The occasional $0.1g$ recorded as gained filter mass is attributed to

the rounding of the digital scale in the laboratory. The filter stops particles below $2\mu m$ so only nanometric particles could possibly pass through. The possibility of nanometric sized particles is discussed in section 6.3, but it is believed there is no formation of such particles given the evidence and the parameters of the system. The reason for the mass increase of a ratio below 1.38 is believed to be due to incomplete oxidation and to the uncertainty of the dispersed quantity. As discussed, incomplete oxidation leaves particles that have not reacted with oxygen and thus maintain their mass as it was initially. This results in the overall mass gain of the products to be less than what is expected for 100% oxidation, that is 1.38 times heavier than initially. The combustion efficiency is discussed in section 6.3, section 6.4 and section 6.5 through three testing procedures: SEM, TGA and XRD. All give clues to the oxidation processes happening in the burner-cyclone system and it will in fact be shown that the initial assumption of one possible oxide form is wrong.

The second reason for a collected mass ratio below the theoretical one is powder not entering the cyclone ducting. A noticeable amount of particles falls down before the cyclone inlet ducting, or remain clogged in the burner assembly. This leads to powder being assumed as dispersed but it in fact never reaches the cyclone, and thus cannot be separated and collected. It is also very likely the iron mass that gets dispersed through the burner is not constant, as measured in the dry runs. If one is not certain about the quantity of powder dispersed, the final mass is not what is expected. For example, consider that 900 grams of powder is dispersed instead of the calculated 1000 grams (according to the dispersion time and rate), and 1242 grams of powder is collected. The collected mass is 1.38 times more than the dispersed one (1242 vs 900 grams), however the user estimates the dispersion at 1000 grams. The ratio recorded is then 1.24 instead of 1.38, as it actually is.

Because the dispersed quantity of powder is unknown to high accuracy, and the combustion efficiency is not yet discussed, the collection efficiency of the cyclonic system then must be evaluated by external factors. Since the ducting and cyclone system is pressure negative and leak-tight, oxidized iron powder cannot escape the system once it enters it after the burner. Iron powder can then accumulate in different areas of the ducting, or it can bypass the cyclone and get stuck in the filter after the cyclone. The most indicative evidence is the lack of powder collected in the filter. There is also no accumulation of powder in the ducting and on the cyclone walls. It can then be concluded that no powder from the burner escapes the cyclone, and that the cyclone separator collects powder at an efficiency of nearly 100%.

6.3 Scanning Electron Microscope

The collected powder is examined on a Scanning Electron Microscope (SEM) by the Materials Engineering department at McGill University. The equipment used is a Hitachi Cold FE SU-8000. Three pair of figures are presented below. All except Fig. 6.10 are from the same batch of powder, sponge iron powder from Tata Steel, that has undergone oxidation in the burner-cyclone system. They are also one of the batches discussed in the Particle Sizing section, section 6.1. The unburnt samples are taken from the batch of powder that is to be introduced in the system. The burnt samples are taken from the cyclone collection bin, once the batch has been burnt.

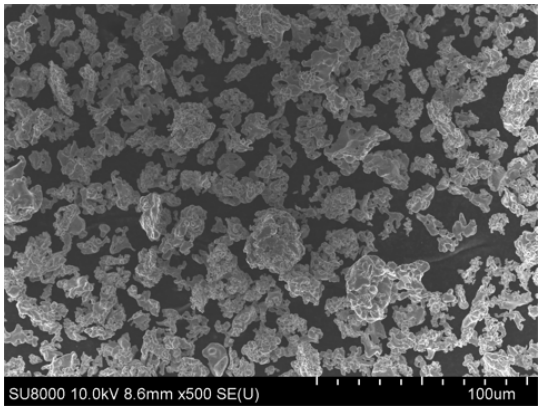

Figure 6.6: SEM on Unburnt Powder Before Going Through the System ($100\mu m$) scale

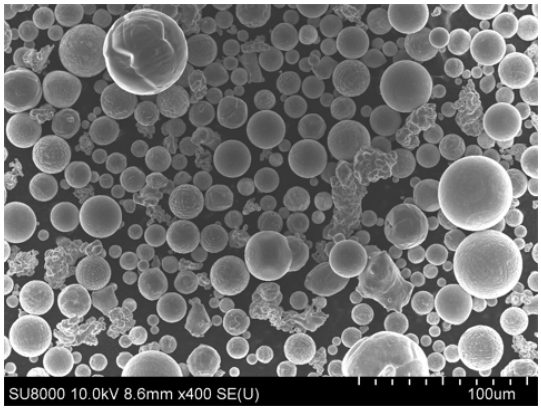

Figure 6.7: SEM on Burnt Powder Collected from the Cyclone ($100\mu m$) scale

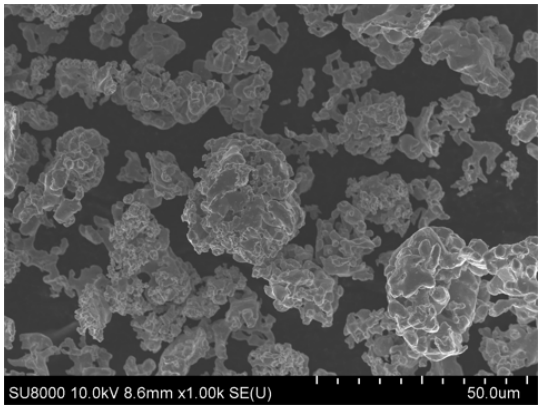

Figure 6.8: SEM on Unburnt Powder Before Going Through the System ($50\mu m$) scale

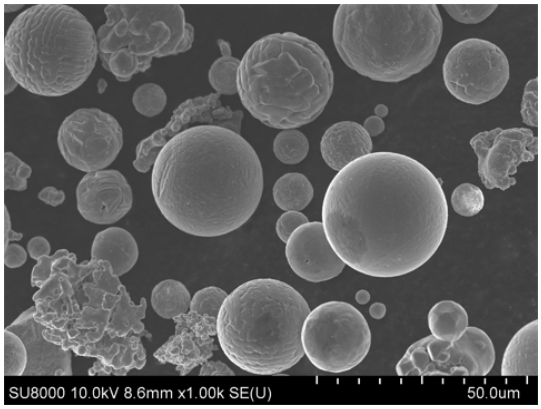

Figure 6.9: SEM on Burnt Powder Collected from the Cyclone ($50\mu m$) scale

The most obvious difference between the burnt and unburnt samples is the shape of the particles. In Fig. 6.6 and Fig. 6.8 it can be seen that the particles examined have an irregular shape. This shape is due to the process used in the fabrication of the iron particles — direct iron reduction yielding

sponge iron. In contrast, the burnt sample seen in Fig. 6.7 and Fig. 6.9 has the vast majority of particles being spherical. This change in morphology is believed to be caused by the temperature treatment of the particles in the iron flame. It is believed that iron particles reach their melting point (about 1800K) while in the turbulent flame. In a soft liquid state, the particles reform in a spherical as they are carried by the gaseous flow. This is due to the fact that they assume the shape with the smallest surface area to volume ratio, i.e. a sphere, in order to minimize surface tension [42]. They then cool down to solidify in that spherical shape.

It is assumed that spherical particles have been at some point completely liquid; that they have melted throughout their full depth. This is explained by the small Biot that they experience during combustion, as discussed earlier. From eq. (1.3), it was found that the value of the Biot number of a spherical particle is determined by $Bi = \frac{Nuk_f}{2k_s}$. It was also discussed that the Nusselt number for a small particle has an empirical value of 2. Since the particles are examined at the moment of melting, the thermal conductivity of air and of iron at 1811K, which are 106 [mW/m K] and roughly 30 [W/m K] [43], are considered for the calculation. Substituting the values in the quation, a value for the Biot number for this experiment is about 3.5E-3. This is much less than one, which is considered to be a small Biot number.

So, if a particle is molten anywhere, it can be safely assumed that it melts throughout. Another evidence for this occurrence is the fact that the collected particles look spherical and dense, unlike the spongy fresh iron powder.

The few particles with irregular shapes seen in the burnt figures could at first sight indicate low or no oxidation levels, since they did not morph into a spherical shape. They could also simply be fresh iron powder that has entered the cyclone collection bin before ignition or in a post combustion cleaning procedure. However, these particles could also have been subject to complete oxidation, at a temperature below the melting point.

An important observation under the SEM is the lack of presence of nano-particles. An example of nanometric sized particle formation can be seen in Fig. 6.10. This is a SEM image from another experiment conducted at the AFL — stabilized iron flame on a hot counterflow burner [5]. Although multiple parameters differ from the burner-cyclone experiment, the counterflow burner products are a reference for nano-particle formation on burnt iron particles. The surface of those spherical particles is not smooth, it is covered in what looks like dust, or snowflakes. Those are the formations of nano-particles caused by a heterogeneous reaction (vapour and liquid phase) on the particle's surface. It can be seen on Fig. 6.11, burnt powder from the turbulent burner, that the surface of

the particles is free of small specks similar to the ones in the counterflow burner experiment. The surface of the burnt powder looks clean and smooth.

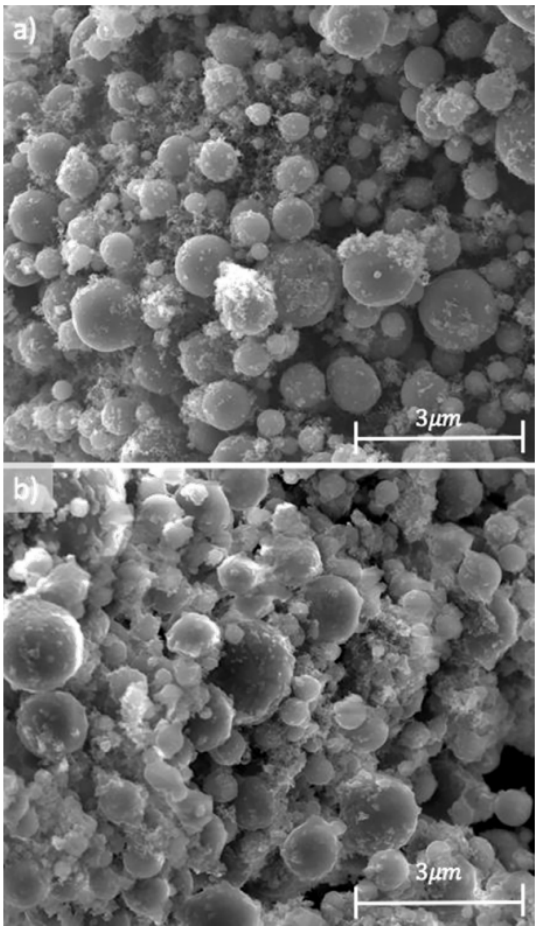

Figure 6.10: Example of Nano-Particle Formations On Burnt Iron Powder [5]

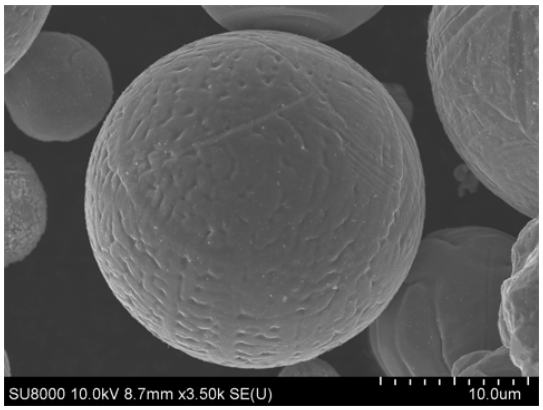

Figure 6.11: SEM on Burnt Powder Collected from the Cyclone ($10\mu m$) scale

The SEM analysis presents promising results in terms of combustion efficiency. The large majority of the iron particles have burned hot enough to reform into spherical particles. However the visual evidence is not conclusive nor quantitative. Although the SEM apparatus also provides Energy-dispersive X-ray spectroscopy (EDS) of the samples, the data is not of great interest. The EDS shows the presence of elements in a sample. However it only estimates their relative abundance to each other and does not provide information on the specific molecules present. For example, a burnt sample contains iron and oxygen, but it is unknown in which quantities and which form (Fe_3O_4 vs Fe_2O_3 for example). Without knowledge of combustion completion rate, a correlation between oxygen and iron levels to oxidation state cannot be made. Powder samples are subjected to two other tests to further understand their oxidation levels and state. Thermogravimetric analysis

(TGA) and X-Ray Diffraction (XRD) are discussed in section 6.4 and section 6.5 respectively.

6.4 Thermogravimetric Analysis

Thermogravimetric analysis, or TGA, is an experimental procedure in which the mass of a sample is monitored and recorded as it is subjected to a temperature profile over time. It is used to promote chemical reactions, phase transitions, absorption, etc, while monitoring the effects on the sample. In the scope of this experiment, the TGA is used to provide oxidation conditions and monitor the mass gain of the sample. Oxidation conditions here mean high temperature and availability of oxygen for a sufficient amount of time. It is known that as iron oxidizes and produces oxides, it gains in mass, as shown in table 6.2. In fact, the TGA is expected to yield information on two different topics – the oxidation completion level of a sample and the formed oxide. They are both indirect results from the recorded mass change of the sample. For example, if pure iron is introduced in the TGA and its mass increases by a factor of 1.43, it means the formed oxide is Fe_2O_3 and it is fully oxidized.

This experiment is conducted in the Structures and Composite Materials Laboratory at the Department of Mechanical Engineering at McGill University. The equipment used is the TGA Q500 from TA Instruments. The equipment is essentially a furnace with a precise scale that can measure very small weight changes. The procedure is to load a sample of powder onto the TGA scale. The target temperature of the furnace, the heating time and the time to reach the target are set. The cool down is not controlled, the furnace simply turns off. The temperature profile of the experiment is shown in Fig. 6.12. The target temperature of 800°C is reached linearly in 20 minutes and kept for 30 minutes. From the instructions of a member from the Structures and Composite Materials Laboratory, this is about the highest temperature that it is reasonable to operate the TGA at. It is also acceptable to promote oxidation.

Five different samples are tested – 3 burnt samples and 2 unburnt samples. The burnt samples are powder taken from the cyclone collection system, after having been burned in the turbulent burner system. Once again, they are the same samples that are previously discussed in other sections of this work. The two fresh powder samples yielded a mass increase of 1.42 times their initial mass. The burnt samples yielded relatively close results, with their masses increasing by factors of 1.035, 1.044 and 1.051. The recorded results are presented in Fig. 6.13.

The first thing to be noted is that the TGA seems to have provided sufficient conditions (temperature and time) for particle oxidation. The mass increase of 42% of the fresh iron powder confirms

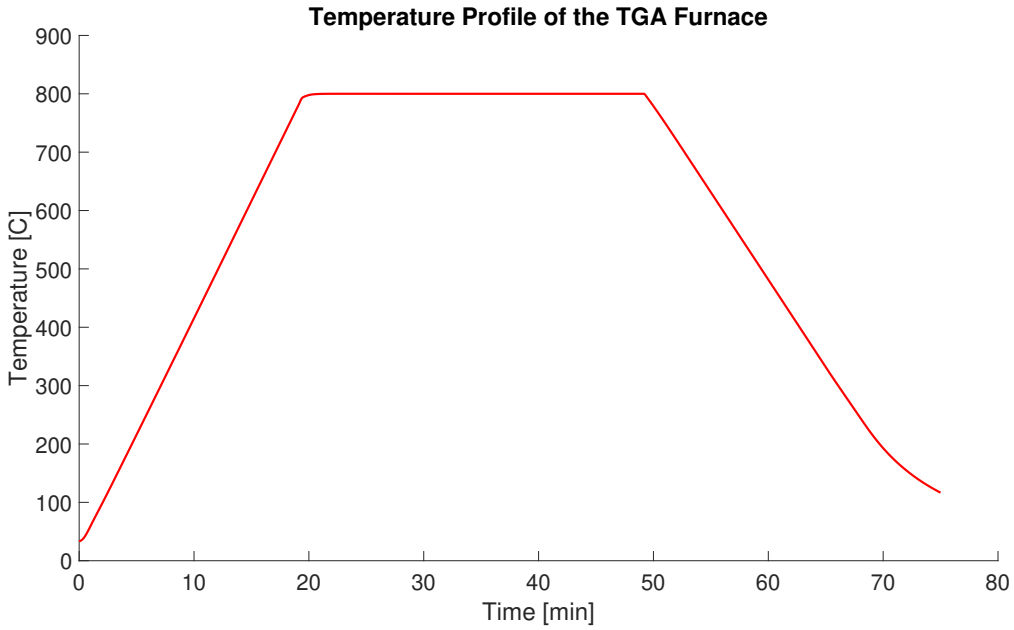

Figure 6.12: Temperature Profile of the TGA Furnace

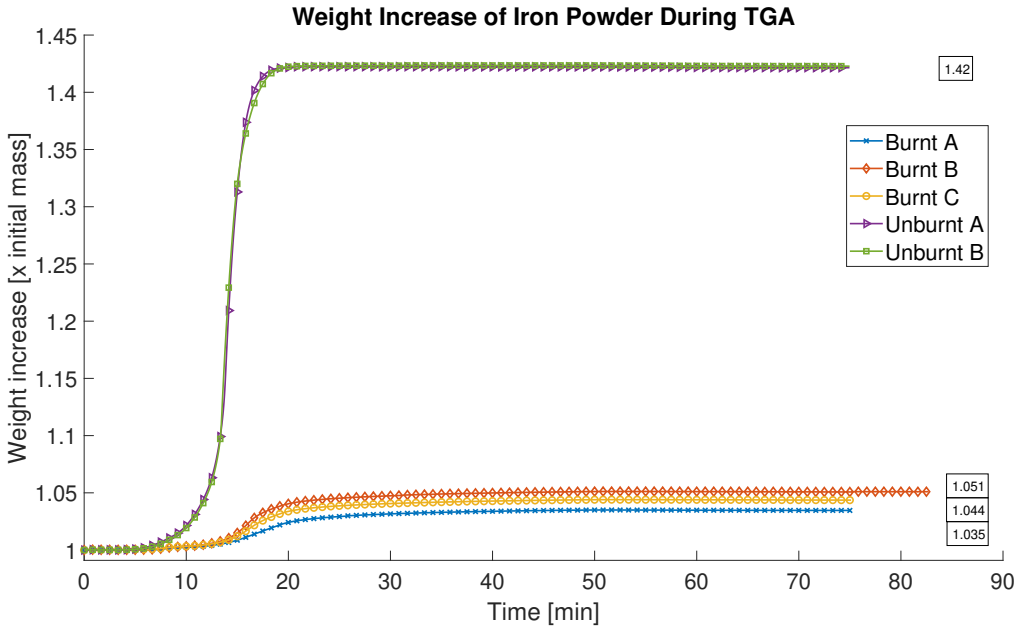

Figure 6.13: Mass Increase of Samples Subject to the TGA Experiment

full oxidation occurs in the TGA conditions, as the mass gain is in agreement with the previously calculated values in table 6.2. After minute 20, all the samples have a constant mass measurement, meaning enough time is given to observe complete reactions. As a preliminary conclusion, it can be said that iron powder is burnt to a relatively high efficiency in the turbulent iron burner, given the operational parameters. However, the exact oxidation completion can only be found by knowing the exact composition of the oxidized sample. This is discussed in section 6.5. Assuming 1.42 times mass increase is the complete oxidation endpoint of all the samples and examining the burnt samples mass increase, it can be concluded that burnt samples A, B, and C are at mass increase ratios of 1.37, 1.36 and 1.35 respectively before being subject to the TGA. In other words, through the turbulent burner cyclone collection system, iron powder samples increased their mass by roughly 35-37%. These values are obtained by reverse calculating the mass increases for the burnt samples based on the complete oxidation assumption. Sample Burnt A is completely oxidized in the TGA with a mass increase of 1.035, bringing it to a total of 1.42 times its initial mass before the AFL burner. Thus, before the TGA, the sample is at $\frac{1.42}{1.035} = 1.37$ times its initial mass. Given the mass increase to form Magnetite is 1.38, it could be concluded that the burnt samples are practically fully composed of Fe_3O_4 oxides, although more evidence is needed. Similarly to the EDS discussion from the SEM experiment, this hypothesis needs to be further studied and verified since it does not show the composition of the samples. The mass increase after the AFL burner can simply be a combination of some particles being fully oxidized to Fe_2O_3 and some not oxidized at all, or anything in between. Although evidence does not show presence of hematite, X-Ray Diffraction is able to give a complete image of the composition of the powder samples.

6.5 X-ray Diffraction

X-ray Diffraction is an experimental procedure in which the molecular structure of a sample can be determined. The beams of x-ray are deflected by the sample in specific directions, depending on the composition of that sample. The resulting observations are then compared to baseline reference values. The XRD analysis was conducted by the McCalla Lab in the Chemistry Department at McGill University.

The particle samples examined under XRD are the pure unburnt iron particles, particles that have burned in the burner-cyclone system, and an unburnt and burnt samples that are subject to a TGA process. The main goal of this experiment is to determine the oxidation rate of the burnt particles. Furthermore, the experiment examines the nature of the oxides. As discussed in

section 6.2, the combustion products are a combination of the different oxidation forms of iron – wustite, magnetite and hematite. The difficulty in determining the oxidation rate solely on mass difference before and after oxidation is that the partial composition of the different oxide states of the sample is unknown. Thus different combinations of oxide presence in terms of quantity, can lead to the same mass increase of an iron powder sample after combustion.

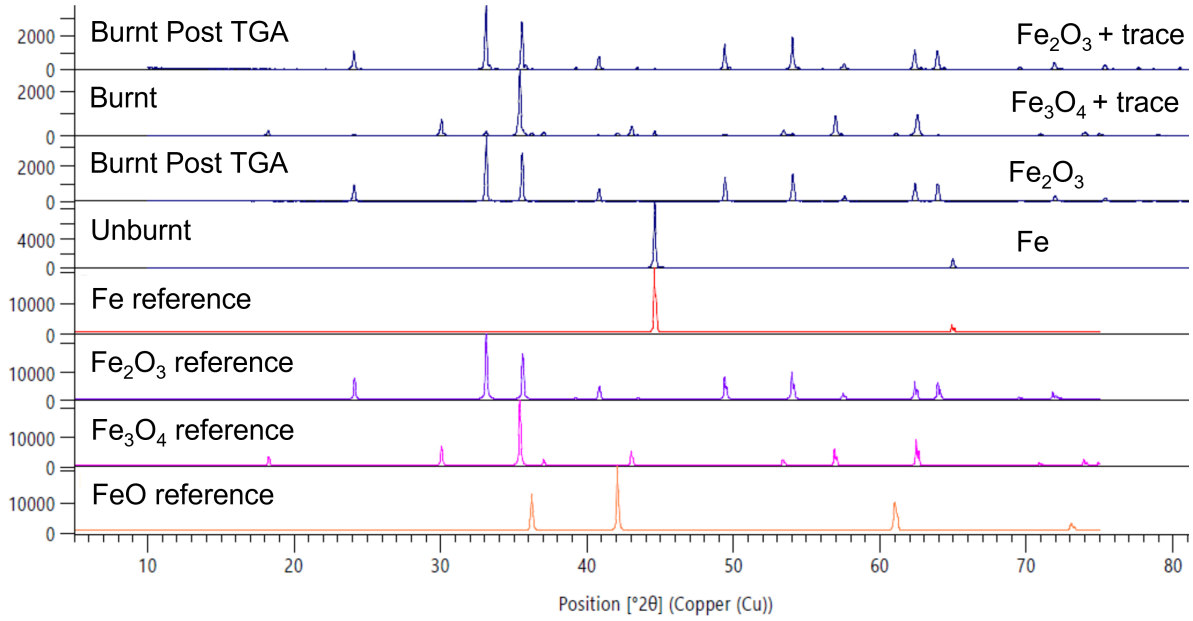

Figure 6.14: XRD Analysis Results

Qualitatively, Fig. 6.14 gives an idea of the examined samples compositions, where "trace" elements could be traces of iron or any other oxide. Looking at the "Unburnt" sample results in the graph, it can be observed that the peaks of the Fe reference coincide very closely with the peaks obtained from the sample. This means that the unburnt, fresh iron powder seems to be completely pure iron Fe. Another sample that is easily comparable to the reference values is the "Unburnt Post TGA" sample. The peaks observed from the XRD correspond directly to the Fe_2O_3 baseline. The TGA sample oxidized completely to Fe_2O_3, hematite, leading to the hypothesis that given a steady high temperature, enough time and oxygen, the final and most complete oxide form of iron is hematite. This is in accordance with the TGA data, as the mass increase of the iron powder is by a factor of 1.42, the same factor to the hundredth as the theoretical one (1.429). Visually the wavelength peaks comparison is not as clear cut for the burnt samples. They seem to be predominantly composed of Fe_3O_4 for the sample straight out of the burner and Fe_2O_3 for the burnt sample after the TGA. This is again in agreement with the previous hypothesis that the burner transforms the iron powder

to magnetite, Fe_3O_4.

The next result of the XRD analysis is the composition by mass of the examined samples.

Table 6.4: Composition of Samples Examined Under XRD in Mass Percentage

Sample Powder	Fe	FeO	Fe_3O_4	Fe_2O_3
Unburnt	100.0	0.0	0.0	0.0
Unburnt Post TGA	0.0	0.0	0.0	100.0
Burnt	2.7	9.5	77.1	10.7
Burnt Post TGA	0.2	0.1	0.0	99.7

Table 6.4 presents the composition by mass percentage in each of the four samples shown in Fig. 6.14. As expected, the unburnt powder is composed only of iron, with all the oxide forms having 0% mass portion of the sample. Once this sample goes through the TGA experiment, it is fully converted to Fe_2O_3, all 100% of its mass. This confirms that the TGA experiment does truly provide conditions for complete oxidation, and that hematite is the most stable and final oxide form. The results from the two burnt samples (pre and post TGA) are more interesting; they have been through the burner-cyclone system. Contrary to the established hypothesis, the "Burnt" sample is not solely composed of magnetite, but is composed of a combination of oxides and a small amount of pure iron. It was previously discussed in section 6.4 that the burn samples collected from the cyclone bin have increased their mass by a ratio of 1.37 compared to the fresh iron powder. It was concluded that they have been fully oxidated to Fe_3O_4, since the magnetite oxide is 1.38 heavier than iron. However this advanced XRD analysis shows that the recorded mass increase by a factor of 1.37 is a numerical coincidence with the calculated value for transformation to magnetite in table 6.2, 1.38 times the initial iron mass.

The breakdown of the products composition can however be used to calculate the combustion efficiency of the iron powder. The combustion efficiency is defined by the ratio of iron that is left unburnt to the total quantity of iron that has been through the burner. It will be discussed later in this section why this assumption might be incomplete, and the following equation provides the lower bound of the combustion efficiency, the minimum.

$$\text{combustion efficiency} = 1 - \frac{m_{\text{FeUnburnt}}}{m_{\text{FeTotal}}} \tag{6.1}$$

Absolute values of iron mass are however unknown. Thus, the values for the burnt sample composition in table 6.4 are used with an arbitrary mass value of the sample, 100 grams. This in turn

means that there are 2.7 grams of pure iron in this sample, and 9.5 grams, 77.1 grams and 10.7 grams of wustite, magnetite and hematite respectively. This is the mass of the products, including the oxygen molecules and the next step is to calculate the mass of iron only in those oxides. For example, using Fe_3O_4, the calculation is as follows:

$$m_{\text{Fe in } Fe_3O_4} = 77.1\% \times 100g \times \frac{1 \text{ mol } Fe_3O_4}{231.53g} \times \frac{3 \text{ mol Fe}}{1 \text{ mol } Fe_3O_4} \times \frac{55.85g}{1 \text{ mol Fe}} = 55.79g$$

From the 100 gram examined product sample, there are 55.79 grams of iron coming from the Fe_3O_4 formed oxide. Repeating this calculation for the two other oxides, the mass of iron due to each of them is shown in table 6.5.

Table 6.5: Mass of Iron From Oxides After Combustion in grams (100 gram sample)

Sample Powder	Non-oxidized Fe	Fe from FeO	Fe from Fe_3O_4	Fe from Fe_2O_3
Burnt	2.7	7.39	55.79	7.48

Using the found values of iron mass in eq. (6.1), it is found that the minimum combustion efficiency for the examined sample is:

$$\text{combustion efficiency} = 1 - \frac{2.7}{2.7 + 7.39 + 55.79 + 7.48} = 96.32\%$$

It is then concluded that more than 96% of the iron dispersed in the AFL burner is oxidized. These results meet and exceed the expectations for the burner performance. However an additional discussion arises about the formed oxides, coming from closer examination of the XRD results in table 6.4. It can be seen in table 6.4 that the "Burnt Post TGA" sample has traces of Fe and FeO despite having been subject to the TGA experiment. In comparison to the "Unburnt Post TGA" sample where all the sample is converted to Fe_2O_3, there is a different mechanism happening in the burner than in the TGA furnace.

It is shown in Fig. 6.15 that Wustite (FeO) is unstable in ambient conditions, temperatures under 570°C. The expected oxidation states of iron at ambient temperatures are magnetite and hematite, depending on the oxidation level during the combustion. It is also known that enough oxygen for full oxidation was provided in the burner-cyclone system, since the cyclone is drawing 4 times the burner air, which is already close to stoichiometric conditions. Additionally, the particles spend enough time in the oxygen-rich environment, both in suspension and in the collection bin of the cyclone.

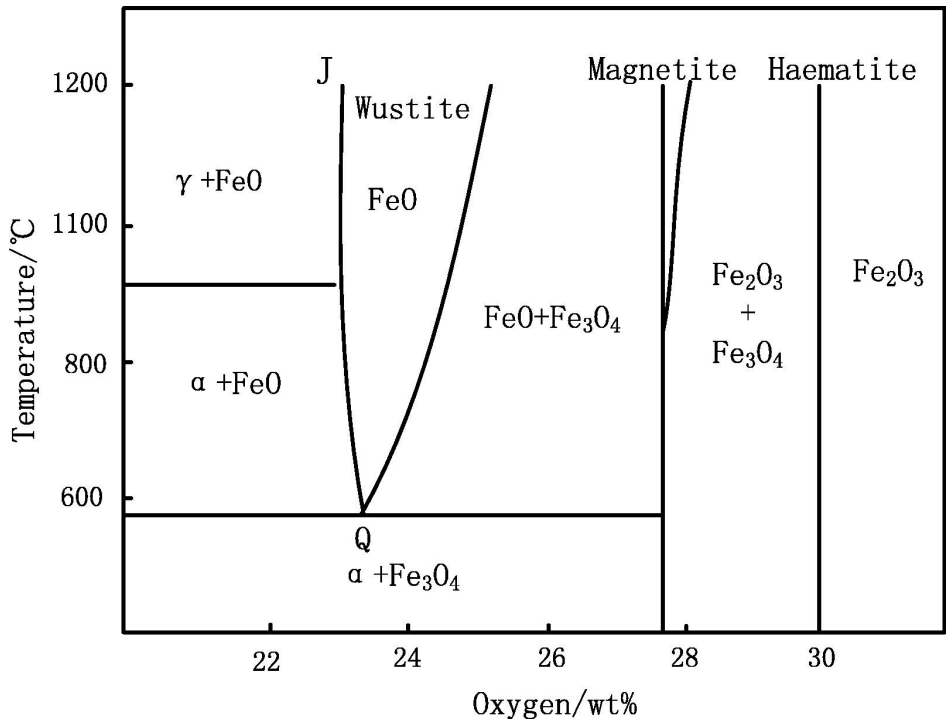

Figure 6.15: Phase Diagram of Iron Oxide Formations[44]

The following hypothesis tries to explain the presence of Wustite in the burnt powder at ambient conditions, as well as the trace iron and Wustite in the post-TGA exposure sample of that powder. The melting temperature of Magnetite is the highest of the melting temperatures of all the oxide forms: Wustite melts at 1650K, Magnetite melts at 1870K and Hematite at 1811K (which is also the melting temperature of Iron). This means that once the conditions to form Fe_3O_4 are met, the conditions to form FeO have also been met. In other words, Wustite should be a passing phase to form other oxides, Magnetite and Hematite, especially considering it is not stable at ambient conditions. A study by Païdassi however records results of iron oxide oxidation that agree with the observations in this work, that is presence of different oxides depending on the oxidation conditions [45]. Païdassi's work confirms that when FeO is maintained between 850-950°C in a TGA furnace for extended periods of time, it is fully transformed to Fe_3O_4 and subsequently fully transformed to Fe_2O_3 [45]. This is in complete agreement with the data shown in table 6.4, where the fresh iron is fully transformed into Hematite in the TGA furnace.

The more interesting conclusions of Païdassi's work come from the experiment of reoxidizing Wustite oxides at high temperatures, around 1500K. As shown in Fig. 6.16, although Wustite was exposed to high temperatures, there is a considerable layer of FeO remaining in the core of the sample. Figure 6.16 shows the microscope image of the sample maintained for 1 min at 1200°C, but the

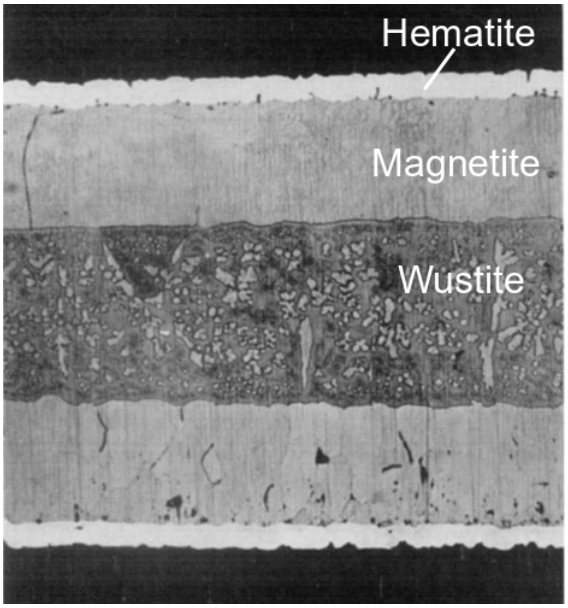

Figure 6.16: Layers of Iron Oxides in TGA Sample Reoxidized at 1200°C For 1 Min [45]

data for samples maintained at that temperature for any amount of time between 1 min and 48 hours is similar, and there is still a thick FeO layer in the sample [45]. A hypothesis for the occurence of this sample could be a kinetically frozen Wustite that cannot continue conversion to hematite or magnetite once it has been frozen.

Studies on the composition of iron and iron during combustion and oxidation are still ongoing. Although it is known and it has been previously discussed that the iron particles experience oxidation while molten, the composition of those particles and the mechanism of combustion are still unknown [46]. Muller et al. explore the composition of iron during combustion at high temperatures, while in a molten state. The research suggests that liquid iron and liquid iron oxides mix during combustion. It can be seen in Fig. 6.17 that there are two possible liquid phases of iron-oxide compositions for temperatures below 2000K, L1 and L2. At 1830K, the L1 phase allows for a very narrow range of oxygen content by w%, from 0 to 0.2, whereas for the same temperature, L2 allows for 22.7 to 26 w% [47]. The exact composition of the liquid sample cannot be known, since the sample is examined once it is frozen and phase change occurs during the cooling. However, there is evidence showing that the liquid state is a composition of the two phases, and it is transitional between them; oxygen levels vary from 0 to about 28 w% and form different oxides. Then when the sample is cooled down, different oxide forms can remain trapped in their state [47].

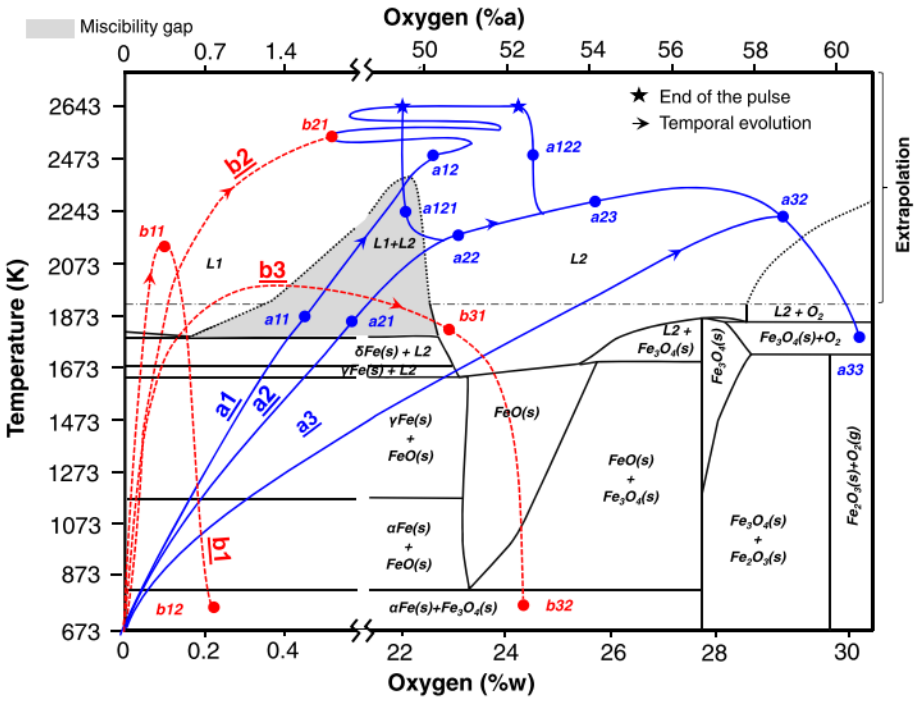

Figure 6.17: Iron–oxygen binary phase diagram at atmospheric pressure, from [48], with proposition of extrapolations at higher temperature.[47]

7 Heat Extraction Experiments

The end-goal for the AFL lab and for the turbulent burner-collection system is to generate electricity from the energy of the iron combustion. As with most fuels, this is done through heat extraction and conversion to mechanical energy. Although heat extraction and electricity production was initially out of the scope of the project, fast progress on the prototypes allowed for the setup and testing of some heat extraction experiments.

Radiative heat transfer is a significant, if not the dominant, heat transfer mechanism in a solid particle flame. Research on coal burners has shown the significance of radiation heat transfer from a powder flame. In a pulverized coal furnace, radiation is the dominant heat transfer mode as 95% of the heat transfer in a coal furnace is due to radiation [49]. There is no research on the heat transfer mechanism in turbulent iron burners, since those do not exist, but an extrapolation can be made from research and experiments of coal burners.

Without going into details, radiation heat transfer is very difficult to model and solve, particularly with a turbulent flow. Radiation heat transfer depends on the emitting and absorbing surface properties, their temperatures and visibility with respect to each other. The turbulent burner

presents a few complications, one of which is the cloud of particles. This results in the fact that particles shadow each other and cannot emit directly onto the outside. A burning particle will partially emit to another particle, which is also burning and hot. Another complication is the fact that similarly to the coal burner, iron particles undergo mass, shape and size changes, as well as variances in optical properties [49].

Since the topic is quite complex and outside of the scope of this project, the most beneficial strategy to obtain a qualitative approximation of the burner heat transfer rate is through an experimental approach.

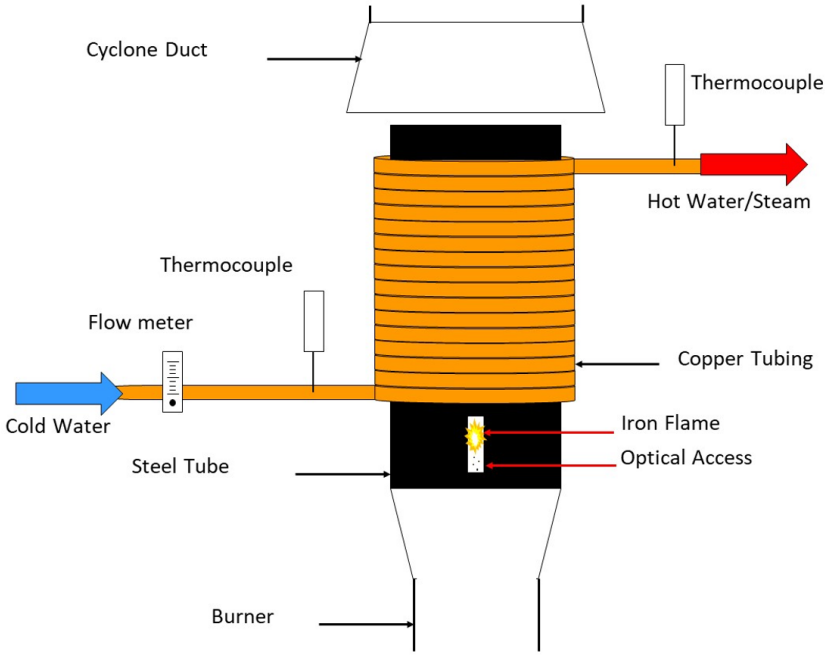

Figure 7.1: Conceptual Drawing of Heat Extraction Experiment

The idea is to surround the turbulent burner flame with a black, non-reflective, highly absorbant surface, for the length of the flame, instead of the usual quartz tube used as a combustion chamber. The radiative heat from the burning particles is absorbed by the black cast iron tube that is installed. A copper tube is then wrapped around the cast iron tube. The heat from the cast iron is transferred to the copper tube by conduction. Inside the copper tube, water flows and heat is transferred through forced convection (the flow of the water). The flow of water is measured, as well as its temperature at the entrance and outlet of the copper coil. This is pictured in Fig. 7.1. Knowing the flow rate (and consequently the mass rate), and the temperature difference, the energy transferred to the water can be calculated, using the heat equation. Although there are in fact a

few heat transfer mechanisms involved in this experiment, radiation, conduction, convection, it is a practically useful experiment since it shows a realistic heat extraction rate from the flame.

$$\dot{Q} = \dot{m}_{\text{water}} C_{P\text{water}} (T_{\text{out}} - T_{\text{in}}) \tag{7.1}$$

The setup experiment is shown in Fig. 7.2 and Fig. 7.3. Water from the local water supply, tap water, is used as the cold source. The temperature of the water is measured with the help of the thermocouples before and after the heating section. The flow of the water is adjusted to reach exactly 100°C. It is measured with the flow meter at the beginning of the coil. Since the inlet temperature varies depending on the tap water temperature, the flow to reach 100°C varies too. A few runs are also executed with an outlet temperature below 100°C, but rather with a higher flow rate. The height of the coiled section is about 30cm and the flame is outputting roughly 10kW.

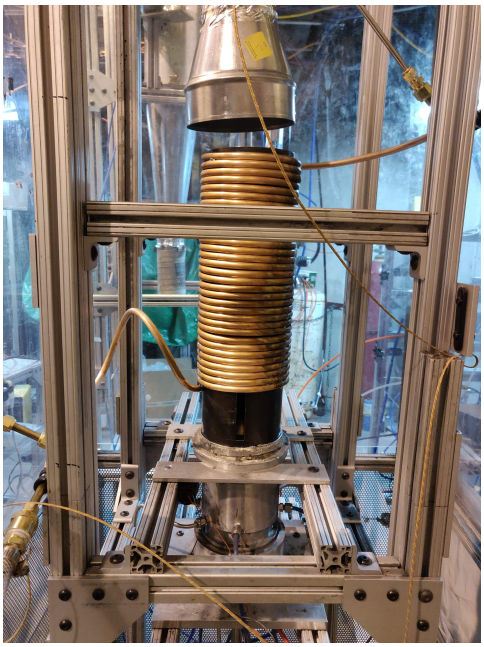

Figure 7.2: Burner With Copper Coil Wrapped for Heat Extraction Experiment

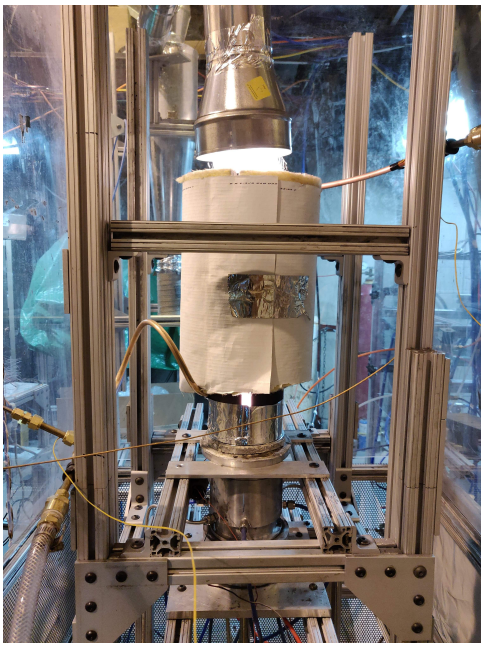

Figure 7.3: Burner With Coil Insulated for Heat Extraction Experiment

With a total of 7 runs, the average energy transferred to the water is 3kW. The lowest heat transfer measured is 2.53kW whereas the highest is 3.96kW. As it can be seen in Fig. 7.4, there does not seem to be a correlation between the flow rate and the heat transfer; the heat transfer rate is relatively constant throughout the different flow rates measured. The highest value of heat transfer does however occur at the highest flow rate and this could be due to a higher convection heat transfer rate because of the higher flow. But even so, it is not significantly larger than the rest of

the data and it can be assumed that about 1/3 of the flame rated power is transferred to the water (3kw out of 10kw). The rest of the heat that is produced by the flame leaves the measurement area in a few different ways. Most of the particles leaving the combustion section are still glowing hot, meaning radiation heat transfer is considerable, and is radiated to the other parts of the system (ducting, cyclone, frame, etc). Some of the heat from the particles heats the gaseous flow around it through forced convection and conduction, which is thrown out of the system in this experiment. Finally, the particles retain heat in them when collected by the cyclone. Sitting in the collection bin, they slowly release that heat to the surroundings by natural convection and conduction.

This heat transfer experiment is simply constructed, and without use of high precision equipment. The main reason for this approach is the time commitment and effort necessary to construct a precise heat transfer experiment, which is outside of the scope of this project. This simple experiment however allows us to show a very conservative result on heat transfer from the flame. This is a baseline result, showing the potential of the iron fuel flame. Additionally, this experiment advances the concept one step further, showing heat extraction is nothing only possible, but quite easy to achieve.

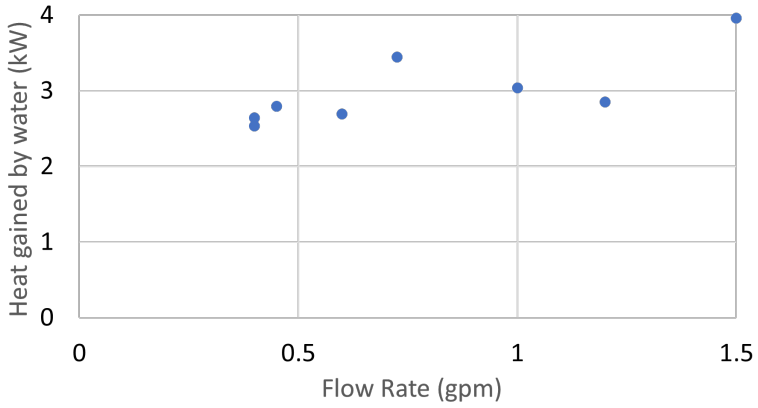

Figure 7.4: Heat Transfer to the Water Flow vs the Flow Rate

8 Second Iteration Cyclone Design

8.1 Motivation

After the success of the first iteration burner-cyclone system, the AFL is motivated to improve on the design. The first version of the cyclone as discussed in section 3.2 is designed to intake four times the flow that the burner supplies, from the ambient air in the room. The purpose is to cool the flow down and increase powder collection. The drawback of this feature is the temperature reduction of the flow. Since the purpose of the burner is to generate heat, this is an undesired side effect from the mark I burner-cyclone system. The main motivation and goals for the mark II cyclone is to improve on that issue. In fact, the second generation cyclone is designed for the flow of the second generation burner, without additional air intake.

The new system has also for a goal to be more compact physically. Minimizing ducting between the burner and the cyclone is the first step toward that goal. This reduces the possibility of powder accumulation in the ducting, reduces heat dissipation and makes the system more compact. The burner design itself is also optimized and compacted. The mark II burner is in a horizontal position to improve dispersion. This leads to an almost direct entry to the cyclone, since there is no need for elbows.

Some design objectives and elements are kept from the first iteration. For example the type of cyclone (cone on cylinder) remains the same since it is tested and meets the requirements. The power output of the burner is also kept as is. The main target for the cyclone remains a complete collection of the burnt products.

8.2 Design

The design process of the second generation cyclone is for the most part the same as for the first generation. The background that supports the design is the same, and the model as well, but it is built upon since the first iteration.

One example of an addition to the model is the inner feed incorporation, which was only added after the design of the first iteration. This effect occurs when the incoming solids concentration exceeds the limit loading, when $c_o > c_{oL}$ [23]. The concept stipulates that any particles that are not immediately separated upon entry have a finer particle size upon reaching the inner vortex. In other words, immediate separation happens for the larger particles. Both the incoming feed and the inner feed then have their own cutoff diameter, x_{50}. The inner feed one is to be found and

the collection efficiency is recalculated including the inner feed concept. The method is relatively similar to the previous x_{50} calculation. Without going into details, it consists of finding the velocity of particles closer to the inner feed, relating it to the flow properties of the inner feed and some empirical relations. The updated predicted GEC for the cyclone is presented in Fig. 8.1. The inner feed incorporation model shows the increased performance of the cyclone, given the high particle loading. In contrast with Fig. 3.3, the high collection efficiency is maintained even for particles below the design cutoff diameter because the cyclone is designed to run at limit loading conditions. The c_o/c_{oL} ratio for the mark II cyclone is around 16, considerably larger than the one of the first iteration (1.13). If the loading ratio proves to be too high, the flow can be diluted with more intake air, and then the loading will be reduced.

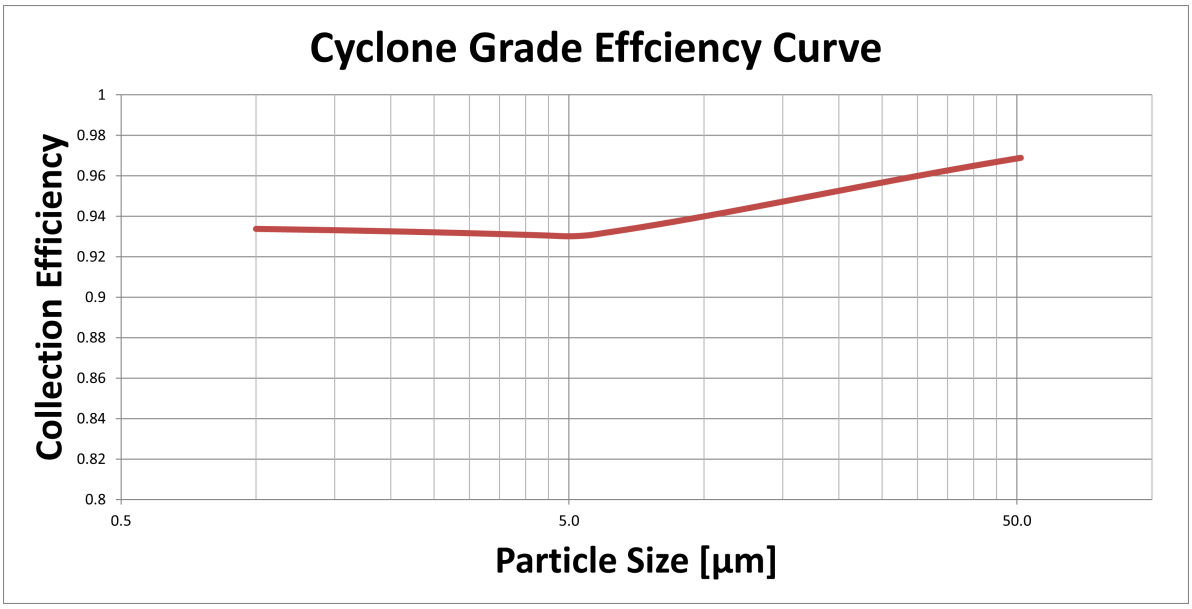

Figure 8.1: Predicted Grade-Efficiency Curve Including Inner Feed Incorporation

The flow rate of the new cyclone is in fact roughly the quarter of the flow rate of the first one – 7.4 CFM (vs 28 CFM). The flow rates of the burner are slightly adjusted since the first design, but remain relatively the same. Since the power rating is kept the same as the first iteration, so is the absolute flow of fuel (iron powder). However, given that the air entering the cyclone is less, this results in a higher particle load for the cyclone. The second iteration cyclone is smaller than the first one, given the lower flow rate through it. Its diameter is $100mm$ and its total height $390mm$.

8.3 Manufacturing

Since the temperature in and around the cyclone is expected to be much higher than the previous one, the cyclone is designed with thicker stainless steel walls ($\frac{1}{2}$in thickness). Thicker walls allow for higher temperatures of the cyclone and the flow inside of it, without compromising its structural properties. Additionally, less heat will be lost to the surroundings when compared to the first iteration (if the temperature of the inside of the cyclone is the same), since there is a higher thermal resistance. Contrarily to the mark I, the McGill machinists are able to manufacture the mark II given its smaller size. The lathes and tools available are long enough to produce the inside conical shape of the lower part of the cyclone. Given this opportunity, the connection type is reverted to the original idea of a flange-gasket type attachment between the cylinder and the cone. The material used is a 7" stock cylinder of stainless steel 304.

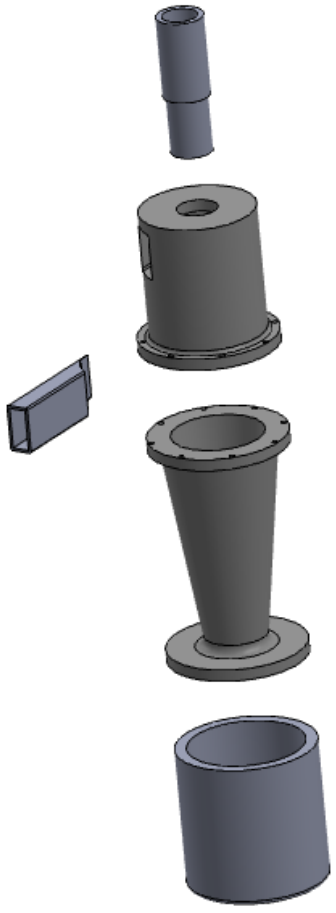

Figure 8.2: Second Iteration of Cyclone Manufacture Drawings

One particularity and an additional manufacturing complexity is the coupling of the inlet and outlet tubes. Those are designed to be welded to the cylindrical part of the cyclone. Stainless steel is particularly difficult to weld and requires specific equipment and steel. The notch seen in the outlet tube mates the tube to the top of the cylinder. The Materials workshop in the Wong building at McGill is able to execute the weld.

The cylinder and the cone are connected together with bolts and nuts that go through both parts. This can be seen in Fig. 8.2. A gasket is cut to match the lip of that connection, and the one between the cone and the collection basket. For the latter, hinged clips are screwed onto the basket and they pull it up to the cone when hooked and tightened to its lip.

8.4 Setup & Testing Procedures

Once again the cyclone is connected in series with the bigger cyclone in the lab. A "Y" damper is added, in a similar fashion and for the same purpose as the first iteration – controlling the flow rate that goes through the cyclone system. One difference with the previous setup is the the cyclone is coupled more tightly to the burner. Although the connection is not sealed for safety reasons, there is no gap for extra air intake, as previously seen. In Fig. 8.3 and Fig. 8.4 the cyclone is pulled away from the combustion section via a railing system, to service and clean the burner.

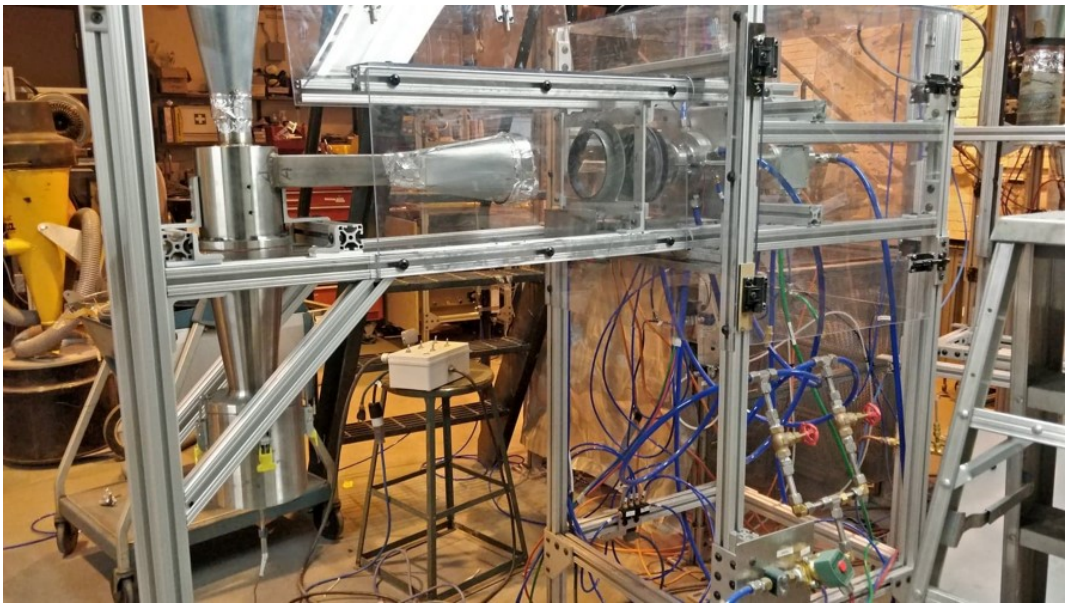

Figure 8.3: Setup of the Mark II Burner-Cyclone System

The testing procedure is practically identical to the first iteration setup. Powder flow is first measured in a "dry" run. The collection bin and the filter after the cyclone are weighed beforehand.

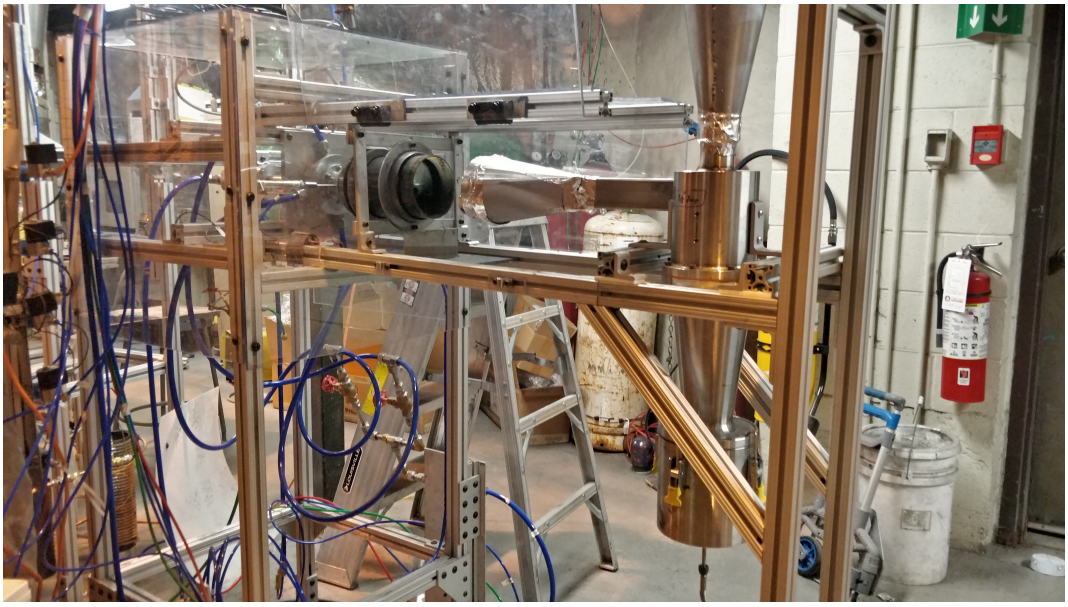

Figure 8.4: Setup of the Mark II Burner-Cyclone System

A flame is then ignited and timed. The weight of the components are compared from before the experiment and thus a conclusion can be drawn. However, this setup is still in the early testing stages, the first of which is stabilizing a flame. Once a flame is stabilized, the parameters of the dispersion system are examined to establish the powder mass flow rate, and the rest of the testing sequence follows. It is already observed that the temperature inside the cyclone is much higher than previously, as expected. Accurate measurements, analysis and evaluation of the system's performance are still to come.

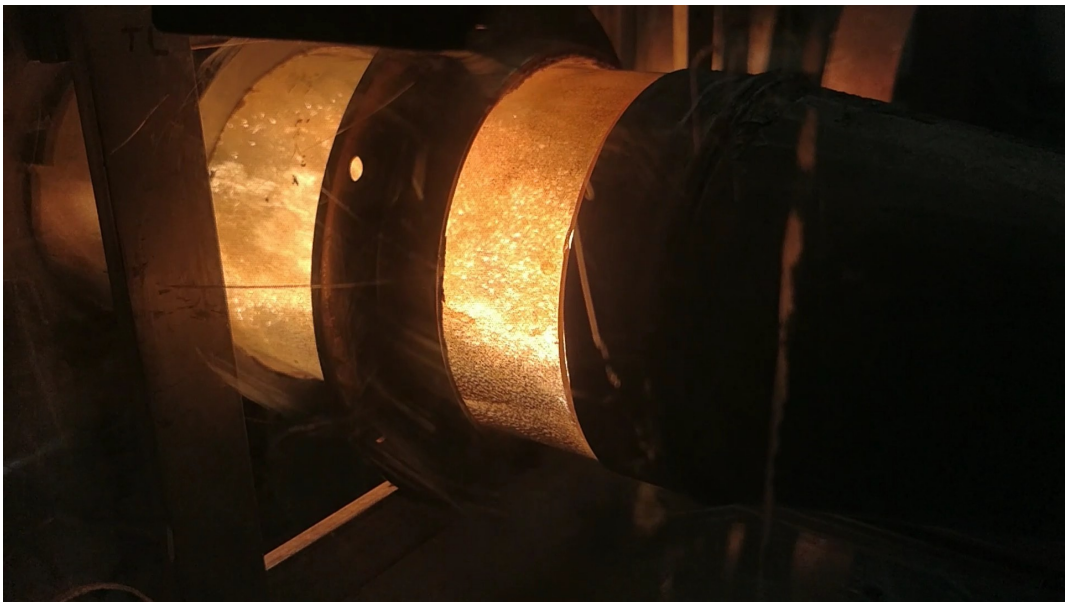

Figure 8.5: Flame Inside the Mark II Burner – Gap With Cyclone Inlet

9 Future Work

This project shows immense potential for the Alternative Fuels Laboratory. A few brand new novel concepts are opened for discussion and research following this project. This is the first system in its kind: a turbulent iron burner with a cyclonic collection that collects all the products. The scope of this project is not on any of the working parameters, which can be explored and further adjusted and improved

Testing the second iteration of the burner-cyclone system is the first task. The collection efficiency needs to be recorded, similarly to the first version of the system. In depth analysis of the products (SEM, TGA, XRD) will quantify the performance of the burner and will possibly show differences with the mark I. A better setup to estimate the amount of powder dispersed is an implementation of laser diagnostics, laser spectroscopy. Furthermore, a temperature profile throughout the system, from the burner to the cyclone outlet can be setup to evaluate heat transfer within the system.

There is also a lot of work to be done in order to fully showcase the iron fuel cycle. Closing the cycle loop in itself is of great importance. Reintroducing the reduced iron oxides, which are pure iron again, will show that iron is truly a renewable fuel. Furthermore, extracting electric power out of the burner-cyclone system will show that iron combustion can easily be used for power generation. It could even perhaps be retrofitted to existing coal burner in power plants.

One concept idea developed following the heat extraction experiment is to split the heat collection

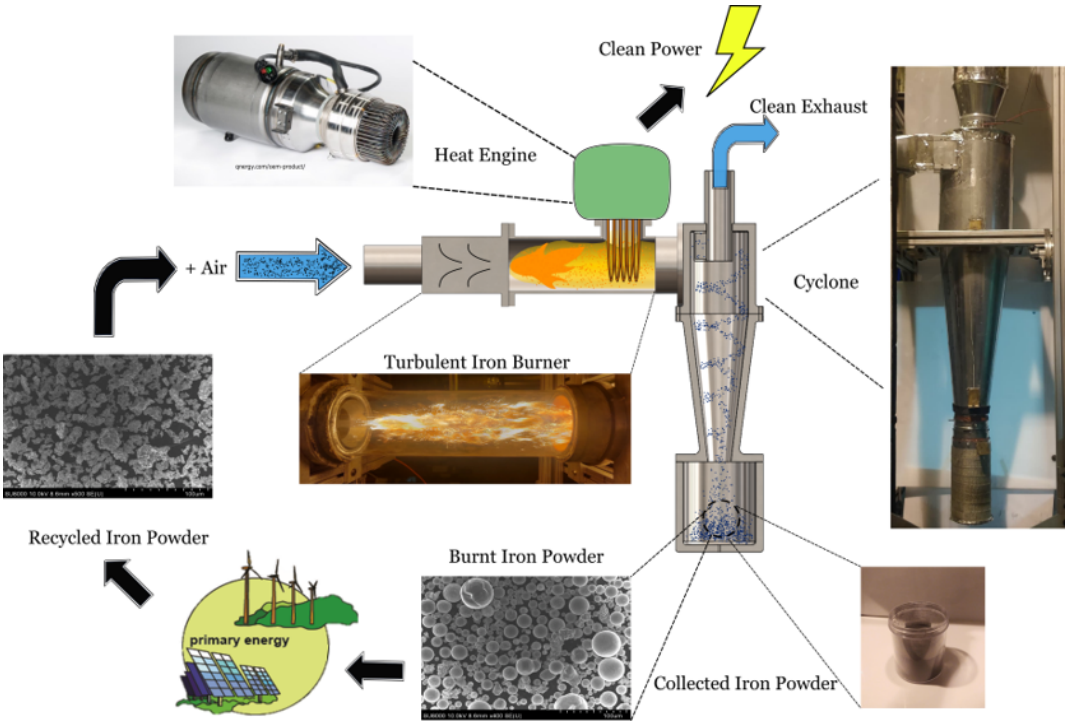

Figure 9.1: Proposed Iron Fuel Cycle

in two zones, one near the flame by being indirect and one later downstream, after the burner. The reasons for this are two: the flow inside the burner is full of hot iron particles. Those are abrasive and will stick to any heat exchanger inserted in the flame. The second reason is that not all the heat leaves through radiation. The leftover heat in the particles and exhaust flow is to be collected as well. A conceptual design of the cyclone is proposed, seen in Fig. 9.2. A cooling jacket is to be added to the cyclone outlet, collection bin and the cyclone body in order to extract the most heat possible out of the hot particles and exhaust flow.

Improving the cyclone's performance for small particles is also an improvement path to be explored. For particles below $5\mu m$, a magnetic field could be used to improve the cyclone's efficiency. Siadaty's modeling work shows that the collection efficiency of $2\mu m$ particles can be improved by nearly 15%, from 82% to 97% [50].

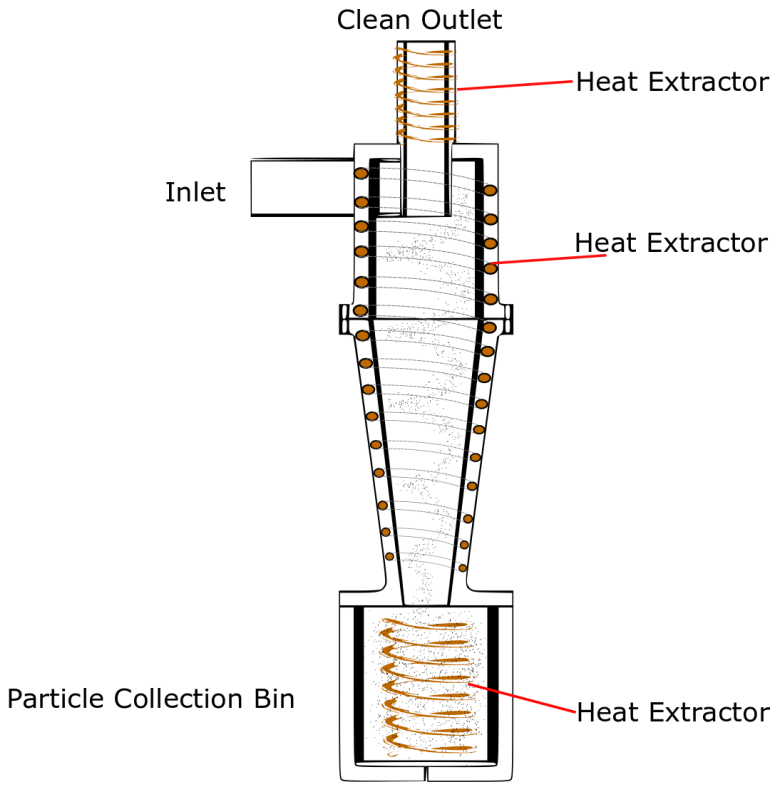

Figure 9.2: Conceptual Design for a Cyclone-Collector and Heat Extractor

10 Conclusion

This thesis has displayed the successful work of the AFL during the past three years: first self-sustained turbulent iron burner with a high-efficiency cyclonic collection system was commissioned, tested and analyzed.

The Master's project began with a goal: a continuous high efficiency collection of the oxidized iron powder coming from the turbulent iron burner. The proper device to achieve the instantaneous collection was then selected through thorough research. A cyclonic separator was chosen because of the system parameters, its ease of manufacture and affordability. Furthermore, its metal body was safe enough to use with the hot flow and metal particles from the burner flow.

The cyclone was designed following decades of documented research and experiments. Since flow inside the cyclone is 3-dimensional and has turbulent components, it is extremely difficult to solve analytically. Most of the modelling equations come from experiments, backed up by theory concepts. The design steps, equations and constants were all combined in an iterative model and the final design was chosen.

Manufactured out of sheet metal, the first iteration of the cyclone was put to the test. The collection

efficiency proved to be excellent, of above 99% by mass. Furthermore the cyclone provided the opportunity to examine the same exact powder that was burned in the turbulent burner. Different analysis was performed on it – SEM, TGA and XRD. Those revealed important information about the system and the process. The oxides formed after the burning process are mostly Fe_3O_4 and there is no trace of nano-particle formation.

A second iteration of the cyclone was designed and manufactured. Testing the mark II system is still a task to be completed. Additionally, reducing burnt powder and reintroducing it into the burner-collection system is to be achieved. Finally, some improvements on the overall system were suggested, particularly with regards to heat and energy extraction from the burner.

References

[1] J.M. Bergthorson et al. "Direct combustion of recyclable metal fuels for zero-carbon heat and power". In: *Applied Energy* 160 (2015), pp. 368–382. ISSN: 0306-2619. DOI: https://doi.org/10.1016/j.apenergy.2015.09.037. URL: https://www.sciencedirect.com/science/article/pii/S0306261915011071.

[2] Jeffrey M Bergthorson et al. "Metal-water combustion for clean propulsion and power generation". In: *Applied Energy* 186 (2017), pp. 13–27.

[3] Jeffrey M Bergthorson. "Recyclable metal fuels for clean and compact zero-carbon power". In: *Progress in Energy and Combustion Science* 68 (2018), pp. 169–196.

[4] Jeffrey M Bergthorson and Murray J Thomson. "A review of the combustion and emissions properties of advanced transportation biofuels and their impact on existing and future engines". In: *Renewable and sustainable energy reviews* 42 (2015), pp. 1393–1417.

[5] Michelle McRae et al. "Stabilized, flat iron flames on a hot counterflow burner". In: *Proceedings of the Combustion Institute* 37.3 (2019), pp. 3185–3191. ISSN: 1540-7489.

[6] "Aluminum-propane-air hybrid flames in a Hele-Shaw cell". In: *Proceedings of the Combustion Institute* 38.3 (2021), pp. 4461–4468. ISSN: 1540-7489. DOI: https://doi.org/10.1016/j.proci.2020.09.017.

[7] Jan Palečka et al. "A new kind of flame: Observation of the discrete flame propagation regime in iron particle suspensions in microgravity". In: *Combustion and Flame* 209 (2019), pp. 180–186.

[8] Jan Palečka et al. "Percolating Reaction–Diffusion Waves (PERWAVES)—Sounding rocket combustion experiments". In: *Acta Astronautica* 177 (2020), pp. 639–651.

[9] Michael Soo et al. "Combustion of particles, agglomerates, and suspensions–A basic thermophysical analysis". In: *Combustion and Flame* 192 (2018), pp. 384–400.

[10] Antje Wadewitz and Eckehard Specht. "Limit value of the Nusselt number for particles of different shape". In: *International journal of heat and mass transfer* 44.5 (2001), pp. 967–975.

[11] Irvin Glassman, Richard A Yetter, and Nick G Glumac. *Combustion*. Academic press, 2014.

[12] Driss Laraqui et al. "Heat recovery and metal oxide particles trapping in a power generation system using a swirl-stabilized metal-air burner". In: *Applied Energy* 264 (2020), p. 114691. ISSN: 0306-2619.

[13] Song Wang, Amy L Corcoran, and Edward L Dreizin. "Combustion of magnesium powders in products of an air/acetylene flame". In: *Combustion and Flame* 162.4 (2015), pp. 1316–1325.

[14] Alex Wright, Samuel Goroshin, and Andrew Higgins. "Combustion time and ignition temperature of iron particles in different oxidizing environments". In: *25th International Colloquium on the Dynamics of Explosions and Reactive Systems*. 2015.

[15] PL Harrison and AD Yoffe. "The burning of metals". In: *Proceedings of the Royal Society of London. Series A. Mathematical and Physical Sciences* 261.1306 (1961), pp. 357–370.

[16] Theodore A. Steinberg, D.Bruce Wilson, and Frank Benz. "The combustion phase of burning metals". In: *Combustion and Flame* 91.2 (1992), pp. 200–208. ISSN: 0010-2180. DOI: https://doi.org/10.1016/0010-2180(92)90100-4. URL: https://www.sciencedirect.com/science/article/pii/0010218092901004.

[17] Ankica Kovač, Doria Marciuš, and Luka Budin. "Solar hydrogen production via alkaline water electrolysis". In: *International Journal of Hydrogen Energy* 44.20 (2019). 9th International Conference on Hydrogen Production (ICH2P-2018), pp. 9841–9848. ISSN: 0360-3199. DOI: https://doi.org/10.1016/j.ijhydene.2018.11.007. URL: https://www.sciencedirect.com/science/article/pii/S0360319918335286.

[18] Noriah Bidin et al. "The effect of sunlight in hydrogen production from water electrolysis". In: *International Journal of Hydrogen Energy* 42.1 (2017), pp. 133–142. ISSN: 0360-3199. DOI: https://doi.org/10.1016/j.ijhydene.2016.11.203. URL: https://www.sciencedirect.com/science/article/pii/S0360319916335522.

[19] Edgar Muschelknautz and Volker Greif. "Cyclones and other gas-solids separators". In: *Circulating Fluidized Beds*. Ed. by J. R. Grace, A. A. Avidan, and T. M. Knowlton. Dordrecht: Springer Netherlands, 1997, pp. 181–213. ISBN: 978-94-009-0095-0. DOI: 10.1007/978-94-009-0095-0_1.

[20] OB Okedere et al. "Usefulness of particulate cyclone in air pollution control". In: *Management of Environmental Quality: An International Journal* (2013).

[21] Friedrich Löffler. "Fundamental Principles of Particle Separation in Fabric Filters". In: *Dust Collection with Bag Filters and Envelope Filters*. Springer, 1988, pp. 1–54.

[22] Arjen Van Nieuwenhuijzen and Jaap Van der Graaf. *Handbook on Particle Separation Processes*. IWA Publishing, 2011.

[23] Alex C. Hoffmann and Louis E. Stein. *Gas cyclones and swirl tubes : principles, design, and operation*. 2nd ed. Berlin ; Springer, 2007. DOI: 10.1007/978-3-540-74696-6.

[24] Anatol Jaworek et al. "Submicron particles removal by charged sprays. Fundamentals". In: *Journal of Electrostatics* 71.3 (2013). Journal of ELECTROSTATICS, Electrostatics 2013 12th International Conference on Electrostatics, pp. 345–350. ISSN: 0304-3886. DOI: https://doi.org/10.1016/j.elstat.2012.11.028. URL: https://www.sciencedirect.com/science/article/pii/S0304388612001428.

[25] Marcel A Lissman. "Dust Collection on Analysis of Mechanical Methods". In: *Chem. and Met. Eng* 37 (1930).

[26] C. B. Shepherd and C. E. Lapple. "Flow Pattern and Pressure Drop in Cyclone Dust Collectors". In: *Industrial & Engineering Chemistry* 31.8 (1939), pp. 972–984. DOI: 10.1021/ie50356a012. eprint: https://doi.org/10.1021/ie50356a012. URL: https://doi.org/10.1021/ie50356a012.

[27] John Dirgo and David Leith. "Cyclone collection efficiency: comparison of experimental results with theoretical predictions". In: *Aerosol science and technology* 4.4 (1985), pp. 401–415.

[28] G. Ramachandran et al. "Cyclone Optimization Based on a New Empirical Model for Pressure Drop". In: *Aerosol Science and Technology* 15.2 (1991), pp. 135–148. DOI: 10.1080/02786829108959520.

[29] David Leith and Dilip Mehta. "Cyclone performance and design". In: *Atmospheric Environment (1967)* 7.5 (1973), pp. 527–549. ISSN: 0004-6981. DOI: https://doi.org/10.1016/0004-6981(73)90006-1.

[30] Melvin William First. "Fundamental factors in the design of cyclone dust collectors". PhD thesis. Harvard University, 1950.

[31] CJ Stairmand. "Pressure drop in cyclone separators". In: *Engineering* 168.4369 (1949), p. 409.

[32] W Barth. "Design and layout of the cyclone separator on the basis of new investigations". In: *Brenn. Warme Kraft* 8.1 (1956), p. 9.

[33] PW Dietz. "Collection efficiency of cyclone separators". In: *AIChE Journal* 27.6 (1981), pp. 888–892.

[34] John Abrahamson et al. "Influence of entry duct bends on the performance of return-flow cyclone dust collectors". In: *Powder technology* 123.2-3 (2002), pp. 126–137.

[35] DI Misyulya. "New designs of devices for a decrease in power consumption of cyclone dust collectors". In: *Russian Journal of Non-Ferrous Metals* 53.1 (2012), pp. 67–72.

[36] Kunihiro Fukui et al. "Effects of clean-air injection on particle-separation performance of novel cyclone with sintered metal cone". In: *Separation and purification technology* 80.2 (2011), pp. 356–363.

[37] Bingtao Zhao, Henggen Shen, and Yanming Kang. "Development of a symmetrical spiral inlet to improve cyclone separator performance". In: *Powder Technology* 145.1 (2004), pp. 47–50.

[38] Khairy Elsayed and Chris Lacor. "Optimization of the cyclone separator geometry for minimum pressure drop using mathematical models and CFD simulations". In: *Chemical Engineering Science* 65.22 (2010), pp. 6048–6058.

[39] Oscar L Sgrott Jr et al. "Cyclone optimization by COMPLEX method and CFD simulation". In: *Powder Technology* 277 (2015), pp. 11–21.

[40] Prashant Singh et al. "Shape optimization of a cyclone separator using multi-objective surrogate-based optimization". In: *Applied Mathematical Modelling* 40.5-6 (2016), pp. 4248–4259.

[41] Zhenhua Ma et al. "New developments in particle characterization by laser diffraction: size and shape". In: *Powder Technology* 111.1 (2000), pp. 66–78. ISSN: 0032-5910.

[42] H. R. Pruppacher and K. V. Beard. "A wind tunnel investigation of the internal circulation and shape of water drops falling at terminal velocity in air". In: *Quarterly Journal of the Royal Meteorological Society* 96.408 (1970), pp. 247–256.

[43] RW Powell, Cho Yen Ho, and Peter Edward Liley. *Thermal conductivity of selected materials*. Vol. 8. US Department of Commerce, National Bureau of Standards Washington, DC, 1966.

[44] Feng Lu et al. "Numerical simulation of iron whisker growth with changing oxygen content in iron oxide using phase-field method". In: *Computational Materials Science* 125 (2016), pp. 263–270. ISSN: 0927-0256. DOI: https://doi.org/10.1016/j.commatsci.2016.09.003. URL: https://www.sciencedirect.com/science/article/pii/S0927025616304414.

[45] J. Païdassi. "Sur l'oxydation du protoxyde de fer dans l'air dans l'intervalle 600–1350°c". In: *Acta Metallurgica* 6.3 (1958), pp. 219–221. ISSN: 0001-6160. DOI: https://doi.org/10.1016/0001-6160(58)90014-2. URL: https://www.sciencedirect.com/science/article/pii/0001616058900142.

[46] Kenji Sato et al. "Metal combustion in high pressure oxygen atmosphere: detailed observation of burning region behavior by using high speed photography". In: *15th Intl Congress on High Speed Photography and Photonics*. Vol. 348. International Society for Optics and Photonics. 1983, pp. 828–832.

[47] Maryse Muller, Hazem El-Rabii, and Rémy Fabbro. "Liquid phase combustion of iron in an oxygen atmosphere". In: *Journal of Materials Science* 50.9 (2015), pp. 3337–3350.

[48] Jean Philibert et al. *Métallurgie: du minerai au matériau*. Dunod, 2013.

[49] Sneh Anjali Varma. "Radiative Heat Transfer in a Pulverized-Coal Flame". In: *Pulverized-Coal Combustion and Gasification: Theory and Applications for Continuous Flow Processes*. Ed. by L. Douglas Smoot and David T. Pratt. Boston, MA: Springer US, 1979, pp. 83–106. ISBN: 978-1-4757-1696-2. DOI: 10.1007/978-1-4757-1696-2_5. URL: https://doi.org/10.1007/978-1-4757-1696-2_5.

[50] Moein Siadaty, Saeid Kheradmand, and Fatemeh Ghadiri. "Improvement of the cyclone separation efficiency with a magnetic field". In: *Journal of Aerosol Science* 114 (2017), pp. 219–232. ISSN: 0021-8502. DOI: https://doi.org/10.1016/j.jaerosci.2017.09.015. URL: https://www.sciencedirect.com/science/article/pii/S0021850217301714.